Check for updates

Chemogenomic Profiling of a *Plasmodium falciparum* Transposon Mutant Library Reveals Shared Effects of Dihydroartemisinin and Bortezomib on Lipid Metabolism and Exported Proteins

Camilla Valente Pires,[a,b] Jenna Oberstaller,[a,b] Chengqi Wang,[a,b] Debora Casandra,[a,b] Min Zhang,[a,b] Jyotsna Chawla,[a,b,c] Swamy Rakesh Adapa,[a,b] Thomas D. Otto,[d] Michael T. Ferdig,[e] Julian C. Rayner,[f] Rays H. Y. Jiang,[a,b] John H. Adams[a,b]

aCenter for Global Health and Infectious Diseases Research, College of Public Health, University of South Florida, Tampa, Florida, USA
bUSF Genomics Program, College of Public Health, University of South Florida, Tampa, Florida, USA
cDepartment of Molecular Medicine, Morsani College of Medicine, University of South Florida, Tampa, Florida, United States
dInstitute of Infection, Immunity and Inflammation, MVLS, University of Glasgow, Glasgow, United Kingdom
eEck Institute for Global Health, Department of Biological Sciences, University of Notre Dame, Notre Dame, Indiana, USA
fCambridge Institute for Medical Research, Cambridge Biomedical Campus, University of Cambridge, Cambridge, United Kingdom

ABSTRACT The antimalarial activity of the frontline drug artemisinin involves generation of reactive oxygen species (ROS) leading to oxidative damage of parasite proteins. To achieve homeostasis and maintain protein quality control in the overwhelmed parasite, the ubiquitin-proteasome system kicks in. Even though molecular markers for artemisinin resistance like *pfkelch13* have been identified, the intricate network of mechanisms driving resistance remains to be elucidated. Here, we report a forward genetic screening strategy that enables a broader identification of genetic factors responsible for altering sensitivity to dihydroartemisinin (DHA) and a proteasome inhibitor, bortezomib (BTZ). Using a library of isogenic *piggyBac* mutants in *P. falciparum*, we defined phenotype-genotype associations influencing drug responses and highlighted shared mechanisms between the two processes, which mainly included proteasome-mediated degradation and the lipid metabolism genes. Additional transcriptomic analysis of a DHA/BTZ-sensitive *piggyBac* mutant showed it is possible to find differences between the two response mechanisms on the specific components for regulation of the exportome. Our results provide further insight into the molecular mechanisms of antimalarial drug resistance.

IMPORTANCE Malaria control is seriously threatened by the emergence and spread of *Plasmodium falciparum* resistance to the leading antimalarial, artemisinin. The potent killing activity of artemisinin results from oxidative damage unleashed by free heme activation released by hemoglobin digestion. Although the ubiquitin-proteasome system is considered critical for parasite survival of this toxicity, the diverse genetic changes linked to artemisinin resistance are complex and, so far, have not included the ubiquitin-proteasome system. In this study, we use a systematic forward genetic approach by screening a library of *P. falciparum* random *piggyBac* mutants to decipher the genetic factors driving malaria parasite responses to the oxidative stress caused by antimalarial drugs. This study compares phenotype-genotype associations influencing dihydroartemisinin responses with the proteasome inhibitor bortezomib to delineate the role of ubiquitin-proteasome system. Our study highlights shared and unique pathways from the complex array of molecular processes critical for *P. falciparum* survival resulting from the oxidative damage of artemisinin.

KEYWORDS *Plasmodium falciparum*, chemogenomics, drug profiles, malaria

1

*P*lasmodium falciparum causes the most severe type of malaria leading to an estimated 241 million malaria cases and 627,000 malaria deaths worldwide in 2020 (1). Of the last remaining frontline antimalarial treatments, artemisinin (ART)-based combination therapies (ACTs) target the symptomatic phase of the disease by killing the parasites during their intraerythrocytic asexual developmental cycle. The exceptional potency of ART against the parasites is well established, but emerging ART resistance (ART-R) (2–6) is leading to increased failures with current treatments. Continued dispersal of ART-R *P. falciparum*, especially to the regions of high endemicity in Africa (7), could have catastrophic consequences, potentially leading to a global resurgence of malaria (8).

The mechanism of action of artemisinin occurs via volatile reactive oxygen species that are created after activation of its endoperoxide bridge by free heme that is released as a result of hemoglobin digestion by the parasite (9–12). The resultant oxidative damage leads to accumulation of damaged and unfolded proteins that overwhelms the parasite's stress response coping mechanisms and eventually leads to parasite death (13–15). Based on this model, the proteasome-mediated degradation pathway is hypothesized to be a major component of the stress responses to artemisinin cytotoxicity, and therefore parasite modulation of the proteasome degradation pathway could be a major contributor to ART-R. Numerous studies support this idea by demonstrating a significant link between artemisinin and the proteasome response mechanisms, suggesting the potential use of proteasome inhibitors with artemisinin to reduce the parasite's ability to tolerate the accumulation of damaged and unfolded proteins (16–18).

A growing body of evidence indicates tolerance of artemisinin by the malaria parasite extends beyond the protein damage response, involving multiple cellular mechanisms that are yet to be unraveled in the complex ART-R phenotype. A number of recent experimental breakthroughs have helped identify some of the other functional changes associated with ART-R, including the K13 resistance mechanism that slows cytostome function, to diminish the available hemoglobin in the food vacuole, thereby slowing release of the free heme (2, 19). Non-K13 mutations implicated in ART-R, such as those of AP-2μ (medium subunit of AP-2 adaptin complex) (20–22), coronin (F-actin-binding protein) (23, 24), falcipain 2 (2, 25–27), and *P. falciparum* phosphatidylinositol 3-kinase (*Pf*PI3K) (28, 29), might also be expected to affect artemisinin susceptibility by altering hemoglobin uptake and trafficking pathways.

The complexity of the ART-R phenotype necessitates additional approaches to provide a more comprehensive understanding of the processes and pathways that can alter artemisinin sensitivity and resistance in *P. falciparum* (30, 31). Functional genomics is a promising approach and has been successfully employed to analyze essential processes in *Plasmodium* and other members of the Apicomplexa (32–35). In this study, we phenotypically screened a library of isogenic *P. falciparum piggyBac* (*pB*) mutants by exposing them to the artemisinin derivative dihydroartemisinin (DHA) and the proteasome-inhibitor bortezomib (BTZ). This allowed us to create chemogenomic profiles and define drug-gene interactions, as we have done previously in other contexts (36–38). As rationalized in previous studies, when exposed to a given drug, *pB* mutants with disruptions in genes that are linked to a drug's mechanism of action will have increased sensitivity and grow poorly compared to mutations in genes not contributing to the parasite's survival under drug stress. Comparing the response of *pB* mutants to the two drugs allowed us to untangle the role of the ubiquitin-proteasome system from the parasite's multifaceted responses to artemisinin and define common and distinct gene sets linked to the DHA and BTZ sensitivity. Transcriptome profiling was used to further define the metabolic pathways related to the stress responses associated with these drug responses and identify dysregulated processes in a sensitive mutant. Furthermore, our results linked *P. falciparum* sensitivity to these compounds with lipid metabolism and protein export, while the regulation of specific factors of the exportome formed a major difference between DHA and BTZ mechanisms of action.
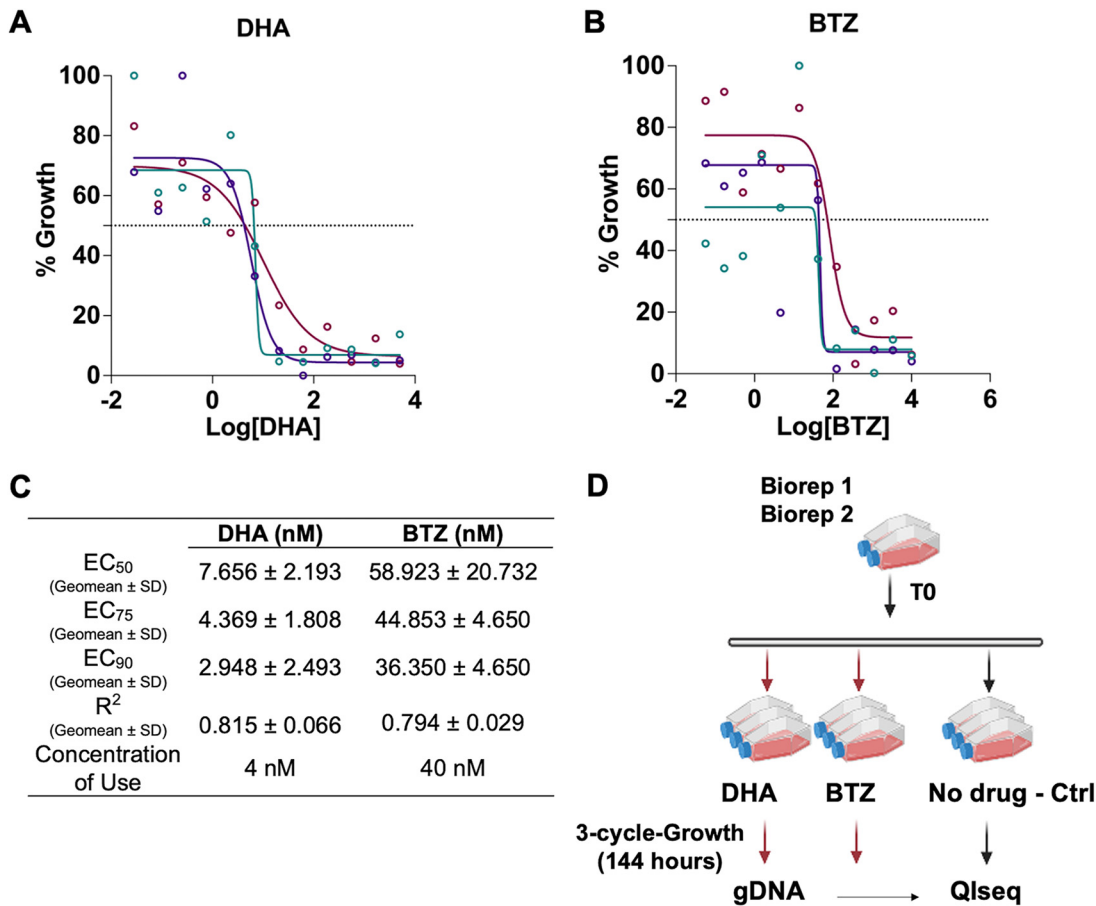
FIG 1 Dose-response curves of (A) dihydroartemisinin (DHA) and (B) bortezomib (BTZ). Standard 72-h drug assays were performed using NF54 (see Materials and Methods); the different colors represent the biological triplicates. (C) Effective concentrations (EC_{50}, EC_{75}, and EC_{90}), R^2 (coefficient of determination) values, and drug concentrations used for the half-K *pB* library drug phenotypic screens; (D) experimental design for DHA and BTZ phenotypic screens. The half-K library ($n = 553$ mutants) was exposed to three cycles (144 h) of continuous drug pressure of sublethal doses of DHA and BTZ. Control flasks were cultured continuously in parallel without drugs. After 144 h of continued drug pressure, the cultures were harvested, and insertion sites were identified by QIseq (quantitative insertion-site sequencing) see (Materials and Methods) (Data Set S1).

RESULTS

Chemogenomic profiling of *P. falciparum piggyBac* mutants. We identified genes linked to responses to the antimalarial drug DHA, an artemisinin compound, and BTZ, a proteasome inhibitor, using phenotypic screens of a *P. falciparum pB* mutant library. The *pB* mutant library was created by single random insertional mutagenesis and included ~600 genetic mutants (here referred to as the half-K *pB* library) with insertion sites in intergenic, untranslated, or exonic regions (see Fig. S1 in the supplemental material). The half-K *pB* library represents ~11% of the *P. falciparum* genome and has a broad representation of Gene Ontology (GO) that is like that of the previously defined saturation library (39). Similarly, there is a broad diversity of GO processes related to artemisinin and stress responses (9, 10, 40), such as virulence factors, exported proteins, lipid metabolism, oxidoreductase activity, phosphatase activity, RNA metabolism, vesicular trafficking, and DNA metabolic processes, such as histone binding (see Fig. S1C and Table S1 in the supplemental material).

The selective pressure for the half-K *pB* library phenotypic screen used sublethal concentrations of DHA (4 nM) and BTZ (40 nM) for three cycles of intracellular growth in parallel with control parasites with no drug exposure (see Materials and Methods) (36, 39, 41) (Fig. 1). Genomic DNA was extracted from each pool before (time zero [T0]) and 1 h after selection (T1), and the relative proportion of mutants present was quantified using quantitative insertion site sequencing (QIseq) (see Materials and Methods)

(41) (Fig. 1B; see Data Set S1 in the supplemental material). Mutants with sensitive and tolerant phenotypes for each drug exposure screen were defined by comparing the growth of each mutant exposed to DHA or BTZ with its growth in the absence of drug selection under ideal culture conditions (see Materials and Methods) (Fig. 1; Data Set S2). The reproducibility of the screening protocol and phenotypes were confirmed by comparing the results from this large-scale screen, to a previously performed small-scale screen of the pilot *pB* library (36) and herein with selected individual *pB* mutant clones treated with DHA and BTZ (Fig. S2).

Mutants with increased sensitivity to both DHA and BTZ were enriched in GO terms described as artemisinin stress responses (9, 10, 40), like homeostasis processes, DNA-repair, phosphorylation, and kinase activity (Fig. 2). Mutants with relative decreased sensitivity to DHA and BTZ (here referred to as tolerant phenotypes) had an expected enrichment in GO processes associated with categories essential for survival under ideal culture conditions (36, 42), such as translation, or a symbiont-containing vacuole (Fig. 2; Table S2).

Mutations that confer increased sensitivity to DHA and BTZ reveal a shared mechanism of action. A set of mutants common to the DHA- and BTZ-sensitive phenotypes were associated with mutations in proteasome-mediated degradation genes. One such mutant had a mutation in PK4 (eukaryotic translation initiation factor 2-alpha kinase [PF3D7_0628200]), which has been previously implicated in the artemisinin mechanism of action and resistance (16, 17, 37, 39, 40, 43) and well-established artemisinin stress responses (10, 16, 18, 40, 44) (Fig. 3). Mutants with mutations in genes for lipid metabolism (45–50), like the StAR-related lipid transfer (PF3D7_0104200), and fatty acid processes (48, 51–56), such as acyl coenzyme A (acyl-CoA) synthetase-7 (ACS7 [PF3D7_1200700]), also showed an increased sensitivity to DHA and BTZ (Fig. 3). These genes have essential roles in lipid transfer (49, 50) and are involved in the transport of intracellular membranes and membranous structures needed for parasite adaptation and remodeling of the host cell (57, 58). StAR-related lipid transfer protein transports phospholipids (e.g., phosphatidylcholine, phosphatidylinositol, phosphatidylethanolamine, and sphingomyelin) between vesicles associated with endoplasmic reticulum (ER) and mitochondrial membranes (49, 50) (Data Set S3, Tab2). Also, this protein is part of the exportome (50, 59, 60), which is the set of *P. falciparum* proteins exported into the infected erythrocyte (59, 61–63). The lipid metabolism processes enriched in the sensitive phenotypes (Data Set S3, Tab2) were shown previously to play a role in homeostatic metabolism (55, 56, 64) and to be essential for asexual blood-stage growth (65), including in the artemisinin responses (64, 66). Additionally, mutations in genes for other exported proteins with vacuolar translocation sequence/host targeting motifs (59, 62), such as proteins targeted to the Maurer's clefts (EMP1-trafficking protein [PTP1; PF3D7_0202200]) and infected red blood cell (RBC) cytosol (PHISTb [PF3D7_0532300], PHISTb/*Pf*G174 [PF3D7_0731300]), also showed increased sensitivity to DHA and BTZ (Fig. 3).
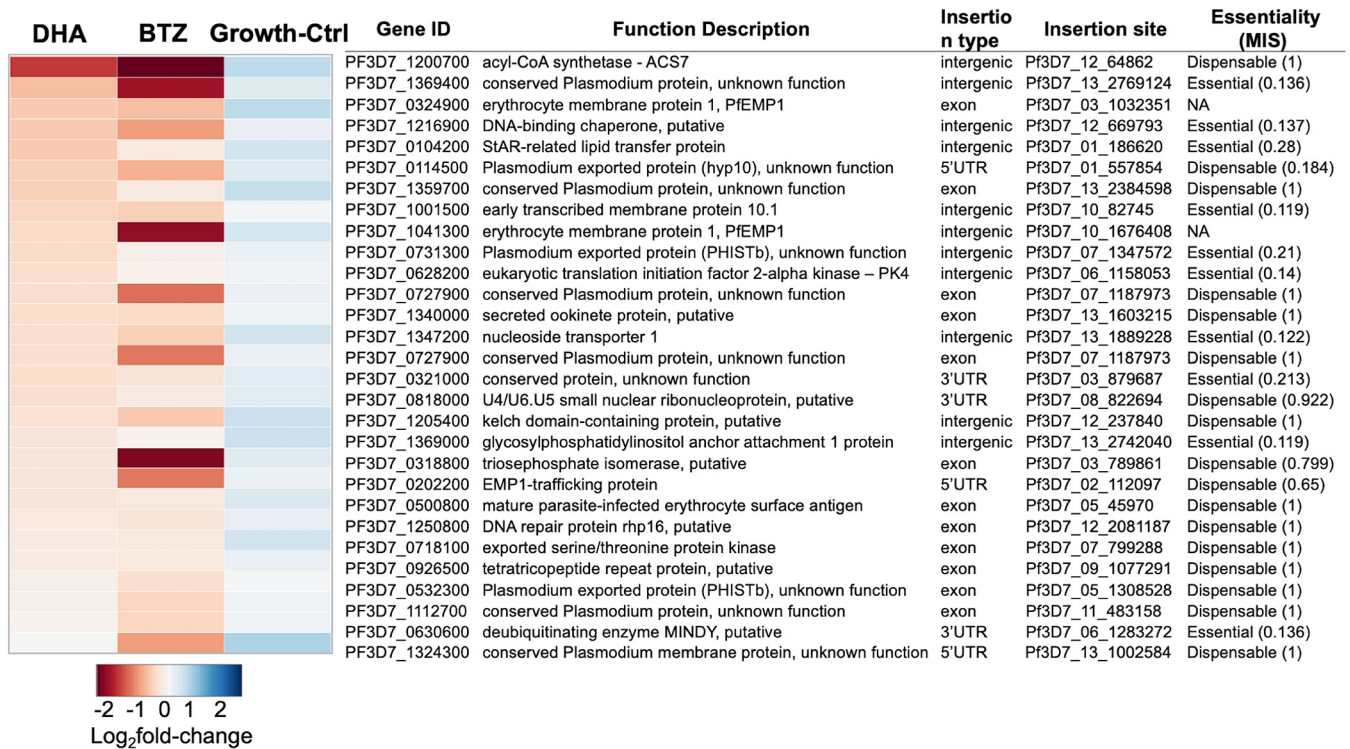
Differential expression of genes in response to DHA and BTZ. To define a broader network of processes and pathways critical for parasite survival under DHA and BTZ treatment, we performed transcriptome sequencing (RNA-seq) for a *pB* mutant (*pB*104 [PF3D7_0104200]) with altered sensitivity to both DHA and BTZ (Fig. 4; Fig. S2 and S3, Data Sets S4 and S5) (36) and for NF54, the wild-type line. We reasoned that this mutant, having altered sensitivity to both DHA and BTZ, would help unravel the common and distinct responses to DHA and BTZ compared to its isogenic wild-type parent.

The clonal line of *pB*104 carries a *piggyBac* insertion in its intergenic region of StAR-related lipid transfer gene (PF3D7_0104200) (36). Another *pB* mutant in the half-K *pB* library has a *piggyBac* insertion in a similar location to *pB*104 and with similarly altered sensitivity to DHA and BTZ (Fig. S4 and S5) (36). The insertion site of *pB*104 is at the PF3D7_01_186648 position, which is only 28 nucleotides (nt) from the insertion site of the uncloned *pB* mutant in the half-K *pB* library at PF3D7_01_186620. The *pB* insertions are localized between two essential genes, PF3D7_0104200 and PF3D7_0104300 (Fig. S4 and S5) (39, 49, 50). StAR-related lipid transfer gene (PF3D7_0104200) is functionally linked to lipid transfer (50) between organelles and between extracellular and intracellular
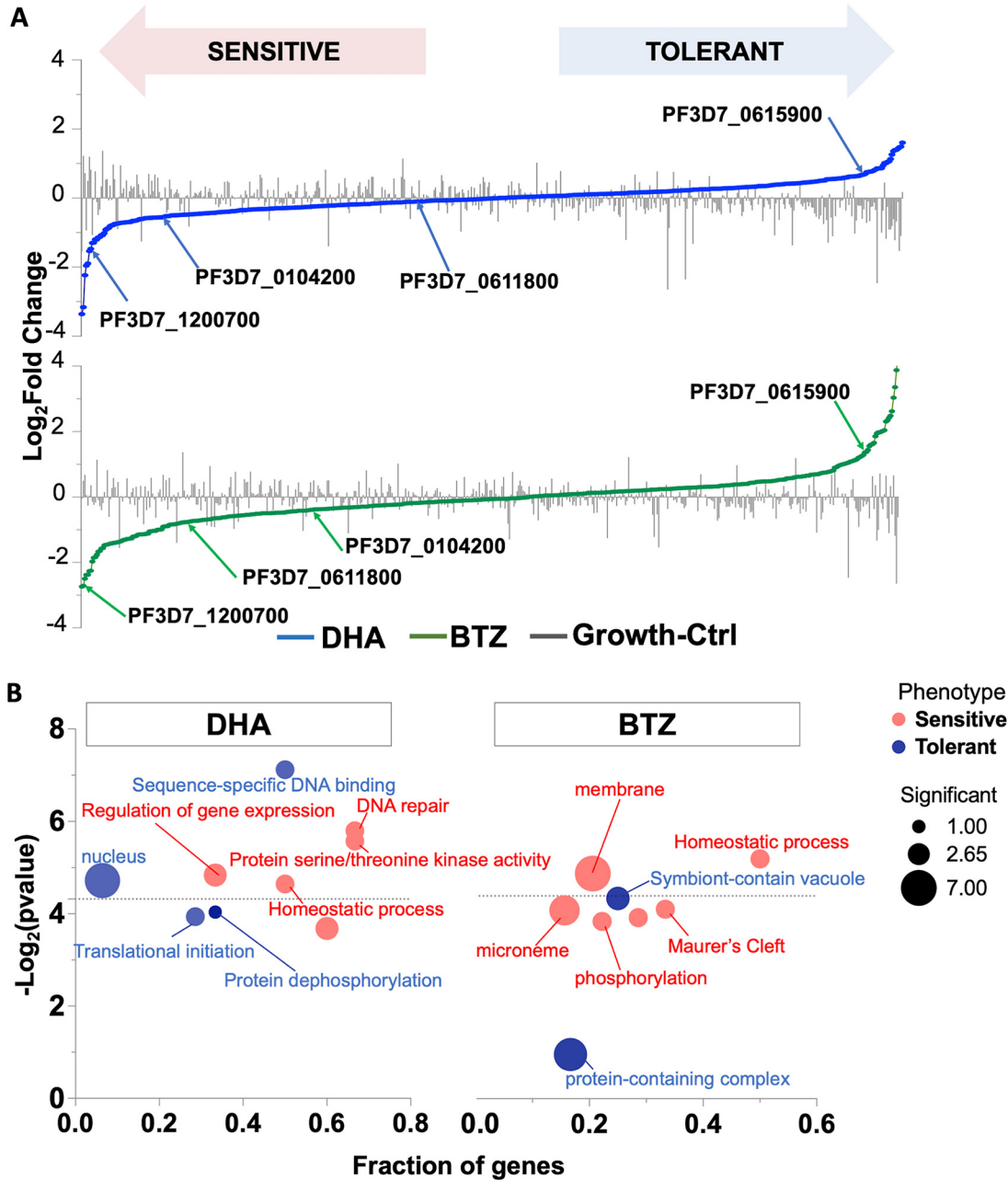
FIG 2 Half-K *pB* library phenotypic screens enable identification of processes underlying the *P. falciparum* DHA and BTZ responses. (A) Schematic plot showing mutant phenotypes to DHA (blue), BTZ (green), and ideal growth conditions (gray bars) identified in the half-K *pB* library. Aliquots of the library were grown in parallel with DHA, BTZ, and under ideal growth conditions. Mutants were assigned phenotypes by established methods (36). DEseq2 was used for log_2 fold change calculations and significance assessments (see Materials and Methods). Mutants are ranked from lower (drug-sensitive; lower quartile; $P < 0.05$) to higher (drug tolerant; upper quartile; $P < 0.05$) log_2 fold change. The mutant's log_2 fold changes in ideal growth are superimposed as a bar plot. Internal redundancy within the half-K and pilot clone *pB* libraries and individual drug pressure results showed that phenotypes were reproducible (Fig. S2). Gene IDs and their products are highlighted in the graph: PF3D7_1200700, acyl-CoA synthetases (ACS7); PF3D7_0104200, StAR-related lipid transfer; PF3D7_0611800, conserved *Plasmodium* protein, unknown function; PF3D7_0615900, phosphatase protein. (B) Gene Ontology (GO) enrichment functional analysis of significant cellular components, molecular function, and biological processes of DHA and phenotypes (sensitive or tolerant) along with their corresponding *P* values (above the dotted line; $P < 0.05$). The GO enrichment was performed for each screen, testing GO terms mapped to genes in the category of interest (sensitive, tolerant, and neutral phenotypes) against a background of GO terms mapped to all other genes in the analysis for each screen (see Materials and Methods) (Table S2). Circles represent the GO term. The circle color represents each phenotype (sensitive, red; tolerant, blue), and the circle size represents the number of significant genes annotated to that term. The fraction of genes represents the number of significant genes annotated to a given GO term in each the category being tested for enrichment (category of interest set) divided by the total number of genes annotated to a given GO term included in the analysis for all categories (background set). Significant terms (two-tailed Fisher's/elim-hybrid test; $P \leq 0.05$) fall above the dotted line.

DHA	BTZ	Growth-Ctrl	Gene ID	Function Description	Insertion type	Insertion site	Essentiality (MIS)
			PF3D7_1200700	acyl-CoA synthetase - ACS7	intergenic	Pf3D7_12_64862	Dispensable (1)
			PF3D7_1369400	conserved Plasmodium protein, unknown function	intergenic	Pf3D7_13_2769124	Essential (0.136)
			PF3D7_0324900	erythrocyte membrane protein 1, PfEMP1	exon	Pf3D7_03_1032351	NA
			PF3D7_1216900	DNA-binding chaperone, putative	intergenic	Pf3D7_12_669793	Essential (0.137)
			PF3D7_0104200	StAR-related lipid transfer protein	intergenic	Pf3D7_01_186620	Essential (0.28)
			PF3D7_0114500	Plasmodium exported protein (hyp10), unknown function	5'UTR	Pf3D7_01_557854	Dispensable (0.184)
			PF3D7_1359700	conserved Plasmodium protein, unknown function	exon	Pf3D7_13_2384598	Dispensable (1)
			PF3D7_1001500	early transcribed membrane protein 10.1	intergenic	Pf3D7_10_82745	Essential (0.119)
			PF3D7_1041300	erythrocyte membrane protein 1, PfEMP1	intergenic	Pf3D7_10_1676408	NA
			PF3D7_0731300	Plasmodium exported protein (PHISTb), unknown function	intergenic	Pf3D7_07_1347572	Essential (0.21)
			PF3D7_0628200	eukaryotic translation initiation factor 2-alpha kinase – PK4	intergenic	Pf3D7_06_1158053	Essential (0.14)
			PF3D7_0727900	conserved Plasmodium protein, unknown function	exon	Pf3D7_07_1187973	Dispensable (1)
			PF3D7_1340000	secreted ookinete protein, putative	exon	Pf3D7_13_1603215	Dispensable (1)
			PF3D7_1347200	nucleoside transporter 1	intergenic	Pf3D7_13_1889228	Essential (0.122)
			PF3D7_0727900	conserved Plasmodium protein, unknown function	exon	Pf3D7_07_1187973	Dispensable (1)
			PF3D7_0321000	conserved protein, unknown function	3'UTR	Pf3D7_03_879687	Essential (0.213)
			PF3D7_0818000	U4/U6.U5 small nuclear ribonucleoprotein, putative	3'UTR	Pf3D7_08_822694	Dispensable (0.922)
			PF3D7_1205400	kelch domain-containing protein, putative	intergenic	Pf3D7_12_237840	Dispensable (1)
			PF3D7_1369000	glycosylphosphatidylinositol anchor attachment 1 protein	intergenic	Pf3D7_13_2742040	Essential (0.119)
			PF3D7_0318800	triosephosphate isomerase, putative	exon	Pf3D7_03_789861	Dispensable (0.799)
			PF3D7_0202200	EMP1-trafficking protein	5'UTR	Pf3D7_02_112097	Dispensable (0.65)
			PF3D7_0500800	mature parasite-infected erythrocyte surface antigen	exon	Pf3D7_05_45970	Dispensable (1)
			PF3D7_1250800	DNA repair protein rhp16, putative	exon	Pf3D7_12_2081187	Dispensable (1)
			PF3D7_0718100	exported serine/threonine protein kinase	exon	Pf3D7_07_799288	Dispensable (1)
			PF3D7_0926500	tetratricopeptide repeat protein, putative	exon	Pf3D7_09_1077291	Dispensable (1)
			PF3D7_0532300	Plasmodium exported protein (PHISTb), unknown function	exon	Pf3D7_05_1308528	Dispensable (1)
			PF3D7_1112700	conserved Plasmodium protein, unknown function	exon	Pf3D7_11_483158	Dispensable (1)
			PF3D7_0630600	deubiquitinating enzyme MINDY, putative	3'UTR	Pf3D7_06_1283272	Essential (0.136)
			PF3D7_1324300	conserved Plasmodium membrane protein, unknown function	5'UTR	Pf3D7_13_1002584	Dispensable (1)

-2 -1 0 1 2
Log$_2$fold-change

FIG 3 DHA and BTZ overlapped sensitive phenotypes. The heat map shows 29 drug-sensitive *pB* mutants for at least one screen (log$_2$ fold change of <0; $P < 0.05$) and with a log$_2$ fold change of >0 for the no-drug growth control, meaning growth under ideal conditions is not compromised. The gene IDs, insertion sites, function descriptions, and essentiality status are based on the mutagenesis index score (MIS) from Zhang et al. (39).

pathways. The ubiquitin carboxyl-terminal hydrolase-1 (UBP1 [PF3D7_0104300]) is associated with the Kelch13-defined compartment (19). In addition, the DHA- and BTZ-sensitive phenotypes of *pB*104 were validated by individual assays with sublethal drug treatments and the ring-stage assay (RSA) (Fig. S2 and S3).

To characterize the transcriptional changes and the dysregulated pathways of DHA and BTZ responses, we compared the differentially expressed genes for NF54 and *pB*104. For that, we defined gene categories based on the relative significance of gene regulation of NF54 and *pB*104 with and without drug exposure (see Materials and Methods) (Fig. 4; Fig. S6). The comparison of transcriptional profiles of wild-type NF54 and *pB*104 revealed distinct responses to DHA and BTZ in terms of the number of differentially expressed genes. DHA had a significant effect on transcription in both parasite lines—the mutant *pB*104 and wild-type NF54 line—with an upregulation of 95 genes and a downregulation of 133 genes (Fig. 4). In contrast, BTZ had a markedly different effect on the parasite lines: 335 genes were upregulated and 201 genes downregulated exclusively in NF54, whereas 295 genes were downregulated and 20 upregulated exclusively in *pB*104 (Fig. 4).

Next, the GO enrichment analysis showed processes enriched for unfolding protein responses to DHA and BTZ were different (see Materials and Methods) (Fig. 4; Fig. S6 and Data Set S6). In fact, activated DHA initiates a series of reactions to alter protein homeostasis by damaging and unfolding proteins, preventing folding of newly synthesized proteins, and inhibiting the proteasome degradation (16). Specifically here, DHA dysregulated genes related to unfolding protein responses (UPRs) (GO:0006986) (Fig. 4C), by upregulating genes coding for chaperone proteins, such as heat shock proteins HSP86 (PF3D7_0708500) and HSP20 (PF3D7_0816500) only in the *pB*104 mutant (Fig. 4; and Fig. S6); and BTZ dysregulated the proteasomal catabolic process protein (GO:0010498) by downregulating it only in NF54, thereby inhibiting proteasomal activation (Fig. 4C; Data Set S6), and the proteasome assembly regulatory particles (GO:0070682) by upregulating them only in *pB*104 (Fig. 4C; Fig. S6), suggesting that a potential overlap between DHA and BTZ responses occurs in the proteasomal catabolic process but not in proteasome assembly.
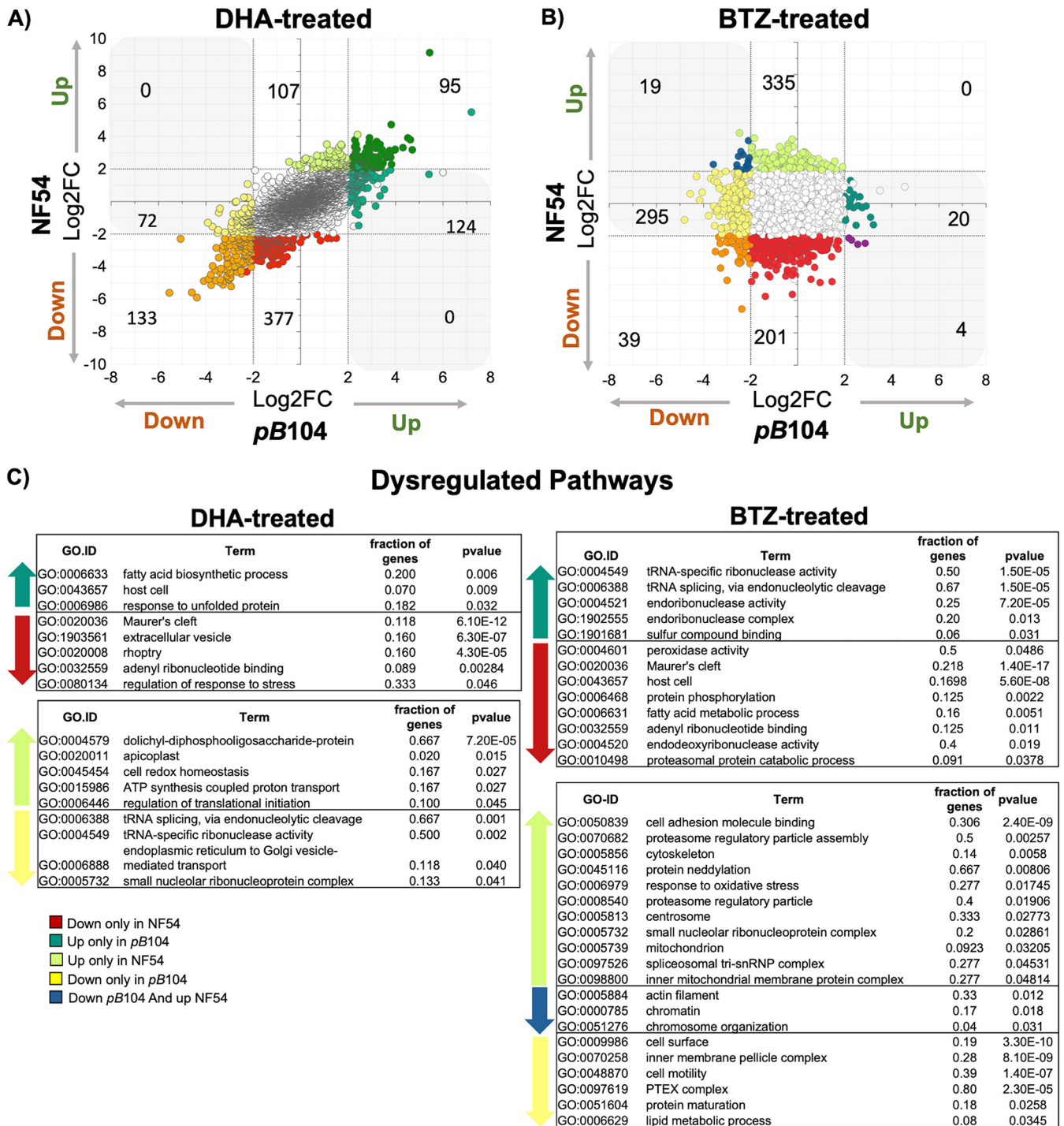
FIG 4 Differential expression of genes reveals parasites with dysregulated expression in the *piggyBac* mutant sensitive to dihydroartemesinin (DHA) and bortezomib (BTZ). Shown is the scatterplot of the log$_2$ fold change of individual genes for *pB*104 (x axis) compared to NF54 (y axis) in (A) DHA and (B) bortezomib. Point color indicates the category of expression genes used to Gene Ontology (GO) enrichment functional analysis (see Materials and Methods) (Data Set S6): white points represent neutral genes (i.e., genes with no significant changes), orange points represent genes downregulated in both parasite lines, red points represent genes downregulated only in NF54, yellow points represent genes downregulated only in *pB*104, light green points represent genes upregulated only in NF54, dark green points represent genes upregulated in both parasite lines, median green points represent genes upregulated only in *pB*104, blue points represent genes downregulated in *pB*104 and upregulated in NF54, and dark reddish-purple points represent genes downregulated in NF54 and upregulated in *pB*104. Shading in gray in the upper left and lower right quadrants signifies genes that are dysregulated—genes with a different direction of regulation comparing *pB*104 and NF54. (C) Relevant GO terms of dysregulated pathways under DHA and BTZ treatment: genes downregulated only in NF54, upregulated only in *pB*104, upregulated only in NF54, downregulated in *pB*104 and upregulated in NF54, and downregulated only in *pB*104. Significant terms were determined by two-tailed Fisher/elim-hybrid test ($P \leq 0.05$) (Data Set S6).

The transcriptome signature also revealed notable similarities in the responses to DHA and BTZ that provoke major dysregulation of genes linked to endosymbiotic organelles and lipid metabolism protein-coding genes. Particularly, the effect of DHA seemed to be more consequential on the apicoplast processes, by upregulating the metabolism-related genes (GO:0020011 and GO:0004579, coding for dolichyl-diphosphooligosaccharide proteins), whereas BTZ affected mitochondrial processes (GO:0005739 and the inner mitochondrial membrane protein complex gene GO:0098800), upregulating them. Notably, these upregulations were observed only in NF54, which were otherwise dysregulated in the sensitive *pB*104 mutant, interpreting as loss function changes (Fig. 4). Importantly, isoprenoid metabolism-related genes and other apicoplast metabolic pathways (67) were downregulated by both DHA and BTZ (Fig. 4; Fig. S5). Specifically, BTZ downregulated 1-deoxy-D-xylulose 5-phosphate synthase (DXS [PF3D7_1337200]) only in NF54, and DHA downregulated 1-deoxy-D-xylulose 5-phosphate reductoisomerase (DXR [PF3D7_1467300]) only in *pB*104. Among lipid metabolism-related processes, DHA upregulated the fatty acid biosynthetic process (GO:0006633) only in *pB*104, while BTZ downregulated fatty acid metabolism processes (GO:0006631) only in NF54. Remarkably, an apicoplast protein-coding gene involved in the fatty acid chain extension step, coding for FabG-3-oxoacyl-[acyl-carrier-protein] reductase (FabG [PF3D7_0922900]) (68), was upregulated by both drugs, with DHA upregulating it only in *pB*104, and BTZ only in NF54 (Fig. 4; Fig. S6).

DHA and BTZ treatment also played roles in the modulation of the pathogenesis-related genes, such as components of the parasite invasion machinery and host cell remodeling/exportome (Fig. 4; Fig. S5 and Data Sets S4, S5, and S6). Maurer's clefts proteins, MAHRP1 (PF3D7_1370300) (69), the serine threonine protein-coding gene FIKK family (PF3D7_0424700) (70), and heat shock protein HSP70-X (PF3D7_0831700) (71, 72) were downregulated only in NF54 in response to both DHA and BTZ (Fig. S6). Of potential functional relevance to these phenotypes, the knockdown of StAR-related lipid transfer and UBP1 proteins (Fig. S5) seems to reduce the transfer of phospholipids between membrane complexes (45–47, 49, 73) and the transport of hemoglobin to the food vacuole (19), respectively. Consequently, this led to the reduction in the global vesicular transport, perhaps by the downregulation of export trafficking processes, such as extracellular vesicles (GO:1903561) downregulated by DHA only in NF54 (Fig. 4C; Data Set S6) (49, 74). Additionally, while DHA dysregulated in *pB*104 the endoplasmic reticulum (ER) to Golgi vesicle-mediated transport process (GO:0006888), BTZ treatment can play a role in the essential core components of the PTEX complex, by downregulating it only in *pB*104 (Fig. 4C; Fig. S6 and Data Sets S4, S5, and S6). The *Plasmodium* translocon of exported proteins (PTEX) complex is formed during invasion, at the same time as parasitophorous vacuolar membrane biogenesis, when the parasite secretes its components. Disruption of any core PTEX component is detrimental to *P. falciparum* viability, as well as in the rodent malaria parasite *Plasmodium berghei*, resulting in dysfunctional protein export and subsequent cell death (75–77).

Genes related to RNA splicing processes were another set of genes dysregulated in the artemisinin-sensitive *pB*104 strain by DHA treatment (Fig. 4), which is consistent with changes observed in ART-R lines (27, 66, 78) and may be functionally related to other changes in RNA metabolism, such as tRNA modification genes reported to be upregulated in K13 mutants exposed to DHA (64). Here, the tRNA splicing machinery was differently regulated in DHA- and BTZ-treated strains, being downregulated only in *pB*104 in response to DHA and upregulated in response to BTZ (Fig. 4C; Fig. S6 and Data Sets S4, S5, and S6).

In summary, our data indicate that the synergic effects between DHA and BTZ are in the canonical parasite responses to artemisinin (10, 16, 40, 44, 64, 79–81), such as protein folding machinery and UPR, DNA repair-related processes, and gene splicing regulation. In addition, our phenotype screens demonstrated the importance of the integrative modulation among organelles' stress responses, including lipid metabolism and the exportome. StAR-related lipid transfer proteins may be responsible for the

Integrated DHA and BTZ responses
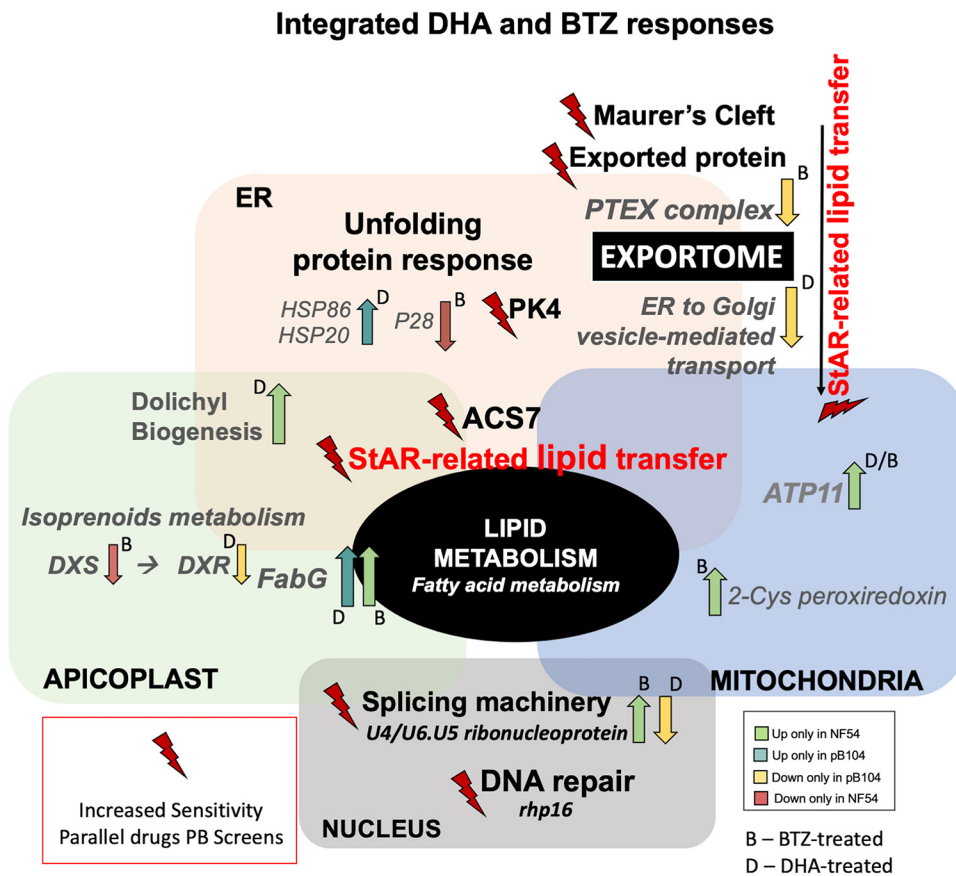
FIG 5 Integrated DHA and BTZ response. All pathways were identified via DHA and BTZ phenotypic genetic screening, and the gene regulation in response to each drug is informed by comparative RNA-seq data where available. DHA- and BTZ-sensitive pathways included the well-known artemisinin mechanism of action-related pathways, such as unfolding protein response (PF3D7_0628200 coding for PK4 [eukaryotic translation initiation factor 2-α kinase]), and DNA repair processes (PF3D7_1250800 coding for DNA repair protein rhp16), as well as gene expression splicing regulation (PF3D7_0818000 coding for the U4/U6.U5 small nuclear ribonucleoprotein). StAR-related lipid transfer (PF2D7_0104200) seems to be the central component of the modulation of lipid metabolism, connecting the organelles' membranes with the exportome components on membrane lipid trafficking, more specifically for PTEX components related to BTZ-treated regulation (PF3D7_1471100 coding for EXP2 [exported protein 2], PF3D7_1116800 coding for heat shock protein HSP101, PF3D7_1436300 coding for PTEX150—translocon component, PF3D7_1345100 coding for TRX2 [thioredoxin 2], and PF3D7_1105600 coding for PTEX88—translocon component). Proteins involved in fatty acid metabolism, ACS7 (PF3D7_1200700) and FabG (3-oxoacyl-acyl-carrier-protein reductase [PF3D7_0922900]), connect its modulation with apicoplast metabolism, more specifically dolichol biosynthesis and isoprenoid metabolism (PF3D7_1337200 coding for DXS [1-deoxy-D-xylulose 5-phosphate synthetases] and PF3D7_1467300 coding for DXR [1-deoxy-D-xylulose 5-phosphate reductoisomerase]), as well as mitochondrial redox metabolism (PF3D7_0802200 coding for 1-CysPxn [1-cys peroxiredoxin] and PF3D7_1209800 coding for ATP11 [ATP synthase mitochondrial F1 complex assembly factor 1]).

connection between the exportome and organelles' metabolism responses, by transferring membranous lipid components (46, 47, 49, 50), and ACS7 connects the organelles' responses by modulation of fatty acid metabolism (51, 82–84). Furthermore, the dysregulated pathways reveal that part of the difference between DHA and BTZ treatment responses is in the regulation of export trafficking, where expression of the PTEX complex components is specifically altered by BTZ (Fig. 5).

DISCUSSION

In this study, we investigated the responses of isogenic *P. falciparum piggyBac* mutants to DHA and BTZ to help elucidate the role of the ubiquitin-proteasome system as it relates to the malaria parasite's response to artemisinin. The chemogenomic profiles from our forward genetic screens combined with transcriptome signatures provided evidence that the different modulation of specific exportome- and organelle-linked lipid metabolism

components represent key differences in the *P. falciparum* response to artemisinin versus ubiquitin-proteasome system. The dysfunction of ACS7 and StAR-related lipid transfer proteins provides a link between the parasite's organellar stress responses and the transport of phospholipids that alter vesicular trafficking and export-related proteins. Importantly, these findings are consistent with analysis of recent ART-R field isolates wherein exported proteins and lipid metabolism, together with organelles' metabolism components, are critical to altering sensitivity to artemisinin's mechanism of action (66, 74, 78, 85).

The results suggest that StAR-related lipid transfer protein connects the exportome to stress response on the organelles. Dysfunction of this gene in the *pB* mutant can explain the increased sensitivity of genes associated with Maurer's clefts and other exported protein-coding genes to DHA and BTZ treatments (Fig. 3; see Data Set S3 in the supplemental material), which might jeopardize the exportome homeostasis and consequently the essential remodeling of the host erythrocyte. Furthermore, the knockdown of StAR-related lipid protein alters the functionality of the lipid metabolism by altering transport of phospholipids (such as sphingomyelin and ceramide [Data Set S3]) to the organelles' membranes (49, 50). The lipid metabolism is an integrative part of the parasite's energy generation, such as the ATP production in the pyruvate and glutamate metabolisms in the mitochondrial functions, which are involved in responses to artemisinin-mediated toxicity (64) and parasite dormancy (55). Thus, the parasite's response seems to redirect the biosynthetic pathways toward new energy sources, providing acyl-CoAs for the tricarboxylic acid cycle metabolism (64). As acyl-CoA synthases catalyze the elongation steps on the fatty acid metabolism II (FASII) *de novo* pathway and for fatty acid metabolism (48, 51, 54, 55, 82–84, 86), we can speculate that fatty acid metabolism components, including ACS7, aid in this redirecting of energy production pathways. Thus, given that StAR-related lipid transfer is part of the exportome of the *P. falciparum* (63, 69), and ACS7 was found as to be potential interactor with SBP1 (skeleton-binding protein 1) in the intracellular trafficking (87), our results show a connection between the exportome and lipid metabolism of endosymbiotic organelles in both of the drugs' mechanisms of action, wherein DHA specifically acts on the apicoplast metabolisms and vesicular trafficking between the ER and Golgi complex, and BTZ acts on the mitochondrial processes and PTEX complex components' regulation (Fig. 4).

Our findings also confirm a synergy between the effects of artemisinin and proteasome inhibitory compounds on the ubiquitin-proteasome system (16, 40), showing increased sensitivity of protein-coding genes involved in this system, such as the gene coding for PK4 (Fig. 3). DHA induces the phosphorylation of eIF2α by PK4, leading to the global translational attenuation (16, 80). Moreover, the transcriptome profiling also highlights specificity of DHA and BTZ regarding the ubiquitin-proteasome system. DHA leads the inhibition of proteasome components required to dispose of toxic aggregates of damaged proteins (16, 43, 78, 88). We demonstrated that DHA regulates the response to unfolded proteins (HSP86 and HSP20) (Fig. 4 and 5) and that BTZ regulates the proteasome activation by downregulating the proteasomal catabolic processes proteins (Fig. 4) and upregulating the PA28 activator (Fig. 4; see Fig. S6 in the supplemental material).

These observations appear related to how resistant parasites use latency caused by repression of general translation to counter artemisinin-mediated toxicity and upregulate the chaperones and proteasome subunit genes necessary to combat the oxidative assault (78). Whereas tRNA processing is upregulated in ART-R isolates (64, 78), and tRNA modifications modulate the translation efficiency of codon-biased transcripts for critical genes (89), here, the tRNA splicing machinery genes were downregulated only in *pB*104 by DHA treatment and upregulated only in *pB*104 in response to BTZ (Fig. 4). We speculate that modulation of artemisinin mechanism of action includes the splicing and translational mechanisms in regulating gene expression. Alternative splicing that has been described for 4.5% of *P. falciparum* genes (90) might be a pathway for modulating responses to drug toxicity. Additional investigation is needed to determine what pathways would play a role in splicing regulation to alter ART sensitivity of parasites.

Our genome-wide screening approach provides a platform for identifying the complex array of genetic factors involved in the parasite's responses to the mechanisms of action to antimalarial drugs. Future studies expanding on our analysis and validating interactive mechanisms of action will further advance our molecular understandings of parasite responses to artemisinin and support the development of efficient drug combination therapies.

MATERIALS AND METHODS

Parasite strains and *pB* mutant library culture maintenance. The wild-type *P. falciparum* NF54, all *pB* mutant lines, and the half-K *pB* library were cultured in 4% hematocrit (O$^+$ erythrocytes from Interstate Blood Bank, Memphis, TN) and 1% Albumax II in RPMI 1640 medium (Invitrogen) supplemented with 50 μg/mL hypoxanthine (Sigma) and 25 mM HEPES (Invitrogen). The culture flasks were grown in an incubator with continuous flow of mixed gas (90% nitrogen, 5% CO$_2$, and 5% O$_2$).

Determination of DHA and BTZ sublethal concentrations. The standard 72-h drug assay was used for the determination of the dose responses of DHA and BTZ. NF54 wild-type line parasites growing in a tightly synchronous culture, using Percoll synchronization for late-stage schizont enrichment (70% to 40% gradient), followed by a treatment with 10% (vol/vol) sorbitol after ~16 h. The ring stages of NF54 line, parental for *pB* mutant lines, at 0.5% parasitemia and 2% hematocrit, were dispensed in plates containing the compounds, serially diluted 1:3 along 12 columns, duplicate per dose, with starting concentrations for DHA of 5 μM and BTZ of 10 μM. The growth response for each compound dilution was obtained by reading the fluorescence generated by DNA intercalating dye SYBR green I (Invitrogen). Plates were analyzed by first reading on the CLARIOstar plate reader for relative fluorescence units (RFU) at the optimal SybrGreen emissions (excitation/emission [Ex/Em] 484-15/528-15). The dose-response curves, with the relevant parameter coefficient of determination (R^2), were plotted and fitted using Prism GraphPad (v.9.3.1). Fifty percent effective concentration (EC$_{50}$), EC$_{75}$, and EC$_{90}$ values were obtained using the same software. Each drug assay was performed in biological triplicate (three independent experiments). The sublethal concentration used this study was ~EC$_{75}$ (geometric mean of all three replicates for each compound): 4 nM DHA and 40 nM for BTZ (Fig. 1A).

Drug *piggyBac* mutant screens. Phenotypic drug screens were performed using an ~600 *pB* mutant library (half-K *pB* library) generated from the saturation library (39). A large-scale *piggyBac* screen pipeline of analysis used in Zhang et al. (36) was adapted for the current work. The pipeline consists of three major steps of quality control: (i) protocols were performed using individual *pB* mutant clones (Fig. S2 and S3), (ii) the methods were adapted for pooled screening using the well-characterized pilot library (which includes the individual *pB* mutant clones assayed individually) (36), and (iii) the methods were then scaled up to screen large pools of uncharacterized mutants, representing the half-K *pB* library (Fig. 1C).

Two independent experiments of screening were performed. In each, several aliquots (at least 2 in each round) of the half-K *pB* library were thawed. From the same thawing, the parasites were split into experimental flasks and control flasks. The control flasks were grown under ideal culture conditions to account for the inherent differences in growth rates of the *pB* mutants in the library (36, 39, 41). A time point zero (T0) sample was immediately harvested. Experimental flasks were continuously exposed to drug pressure at sublethal doses: 4 nM DHA and 40 nM for BTZ for three growth cycles (144 h). Use of higher doses, such as EC$_{50}$ or clinical therapeutical doses (700 nM), results in the death of mutants in the pool that greatly diminishes the broader GO representation of the library. As the artemisinin is metabolized rapidly and eliminated within hours (91), old medium was replaced with new medium, and drugs were carefully added every completed 24 h, at due concentrations, during the screening experiment. Parasitemia of all cultures was maintained at 2% during the experiment. The control flasks were cultured continuously in parallel at 37°C without the drug. The parasites were harvested immediately after three growth cycles for genomic DNA extraction and phenotype analysis via QIseq (41).

Phenotype identification and quantification. The QIseq methodology was used to identify and quantify *piggyBac* mutants using a modified Illumina sequencing technology and custom library preparation by sequencing from the 5' and 3' ends of the *piggyBac* transposon into the flanking genome sequences, and the number of sequence reads per insertion site reflects the relative abundance of each mutant (41) (Data Set S1, Tab2). DEseq2 (41), from R, was used to normalize and calculate fold change between drug treatments (DHA and BTZ) (log$_2$ fold change for drug versus control) and no-drug growth control (log$_2$ fold change at T1 for the no-drug control versus the T0 no-drug control). The sensitive mutants present a log$_2$ fold change of <0 and the tolerant log$_2$ fold change of >0, with a P value of <0.05 indicating significance. A log$_2$ fold change of the growth control of >0 (zero) means growth under ideal conditions is not compromised (36, 41) (Data Set S2). High correlations between biological replicates were observed (Fig. S7).

Sublethal dose drug exposure and ring survival assay of individual *pB* mutants' growth. Phenotype methods for the half-K *pB* library drug screens had been validated previously in small-scale screens (36) and here in growth assays of individual *pB* mutant clones. The wild type (NF54) and *pB* mutant clones associated with StAR-related lipid transfer (*pB*104 [P3D7_0104200]), phosphatase protein (*pB*3 [PF3D7_0615900]), and conserved *Plasmodium* protein of unknown function (*pB*15 [PF3D7_0611800]) were grown with sublethal dose drug exposure and used in the ring survival assay (RSA) (Fig. S3). For the sublethal dose drug exposure (Fig. S3A and B), parasite lines were synchronized in the ring stage by treatment with 5% (vol/vol) sorbitol at 4 h postinvasion (HPI) and diluted down to 0.5% parasitemia at a 4% hematocrit in standard culture medium (described above). Experimental cultures were exposed to 96 h of

continuous drug pressure at the sublethal doses: 4 nM DHA and 40 nM BTZ. Controls were cultured continuously in parallel without drug. The medium, containing a fresh dilution of each drug, was changed every day. Giemsa smears were taken every 24 h until 96 h. The parasitemia was estimated by counting, at a ×100 magnification under immersion oil, the number of infected red blood cells (RBCs) containing viable parasites in a total of at least 10,000 RBCs. Each sublethal dose assay was performed in duplicate.

The RSA (Fig. S3C) was performed as previously described (92; https://www.wwarn.org/tools-resources/procedures/ring-stage-survival-assays-rsa-evaluate-vitro-and-ex-vivo-susceptibility). Briefly, parasites were thawed and maintained in culture until reaching the 2 to 4% majority ring stage for sorbitol synchronization. Sorbitol synchronization was again performed 48 h later, depending on parasite development and the stages at the time of sorbitol treatment. After 30 h of culture (majority late schizont stages), cultures were subjected to Percoll synchronization for late-stage schizont enrichment (70% to 40% gradient). The culture was incubated (37°C, mixed gas) for exactly 3 h. Thin smear slides were then taken to evaluate the proportion of ring stages (>0.5%), cultures were incubated with sorbitol, and parasitemia was adjusted to 0.5% at a 2% hematocrit. Tightly synchronous ring-stage parasites at 0 to 3 HPI were then incubated with 700 nM DHA for 6 h, after which the drug-containing medium was washed out, and the parasites' cultures were allowed to grow into the next invasion cycle for 66 to 72 h. The RSA was performed in triplicate. Giemsa smears were taken, and the parasitemia was estimated by counting, at ×100 magnification under immersion oil, the number of infected red blood cells (RBCs) containing viable parasites in a total of at least 10,000 RBC.

Comparative RNA-seq between wild-type NF54 and the drug-sensitive *pB*104 mutant parasite line in response to DHA and BTZ. The RNA-seq experimental design is outlined in Fig. S8. Two independent experiments were performed. Briefly, cultures of wild-type NF54 and sensitive mutant *pB*104 were sorbitol-synchronized 3× to highly synchronous rings, the parasites at time point zero (T0) were harvested and then split equally into experimental (drug exposure) and control (no-drug) flasks. Flasks of each parasite line were then exposed to 96 h of continuous drug pressure at sublethal doses of DHA (4 nM) and BTZ (40 nM), the same concentrations used for the half-K *pB* library screens. Control flasks were cultured continuously in parallel at 37°C without drug. Cultures were maintained under the normal conditions of culture (described above in "Parasite strains and *pB* mutant library culture maintenance"). After 96 h, the RNA was harvested simultaneously from all conditions for RNA-seq as in reference 81. Parasitemia was verified daily by Giemsa smear. RNA-seq was performed in-house on an Illumina NextSeq v.2.5 mid-output 300-cycle, Trueseq reagent kit.

RNA-seq data analysis. RNA-seq reads from each sample were aligned to the *P. falciparum* reference genome (PlasmoDB v.47). A maximum of one mismatch per read was allowed. The mapped reads from HISAT2 (93) and SAMtools (94) were used to assemble known transcripts from the reference, and their abundances were estimated using Feature Counts (95). DEseq2 was using to normalize fold change calculation (drug treated versus control) and significance assessment of differentially expressed genes. The correlations between biological replicates are outlined in Fig. S9. A $\log_2$ fold change of >2 and adjusted P value (Padj) of <0.01 classified genes as significantly upregulated for the drug treatment; a $\log_2$ fold change of less than −2 and Padj of <0.01 determined genes as significantly downregulated in response to drug treatment (Data Sets S4 and S5).

Gene Ontology. All Gene Ontology (GO) enrichment analyses were performed testing GO terms mapped to genes in the category of interest against a background of GO terms mapped to all other genes in the analysis. The GO term database was created from the latest curated *P. falciparum* ontology available from PlasmoDB (accessed November 2021), using R package pfGO (v.1.1) (96; https://github.com/oberstal/pfGO), wherein the enrichment was assessed via a weighted Fisher/elim-hybrid P value of ≤0.05 (topGO; R package v.2.46.0) (97).

For the GO enrichment analysis of all genes disrupted in the half-K *pB* library (Fig. S1C), the tested categories of interest were "genes disrupted in the half-K *pB* library" versus "genes disrupted in the saturation library" (36) (Table S1).

For GO enrichment analyses of the phenotype of each screen (DHA and BTZ), categories of interest were "sensitives," "tolerant," and "neutral" (Fig. 1B; Table S2).

For GO enrichment analysis of RNA-seq transcriptional data, we assigned categories for significant differentially expressed genes based on the relative gene abundance of wild-type NF54 and the *pB*104 mutant. For example, "upregulated-NF54-only" included genes significantly upregulated only in NF54, "downregulated-NF54-only" included genes significantly downregulated only in NF54, "upregulated-*pB*104-only" included genes significantly upregulated only in *pB*104, "downregulated-*pB*104-only" included genes significantly downregulated only in *pB*104, "downregulated-NF54-and-*pB*104" included genes significantly downregulated in both lines, "upregulated-NF54-and-*pB*104" included genes significantly upregulated in both lines, "down-*pB*104-and-up-NF54" included genes significantly downregulated in *pB*104 and upregulated in NF54, and "up-*pB*104-and-down-NF54" included genes significantly upregulated in *pB*104 and downregulated in NF54. All other genes without significance for differential expression were classified as neutral (Fig. 4; Data Set S6).

Malaria Parasite Metabolic Pathways enrichment analyses. Complementary to GO-enrichment, pathway enrichment analyses were performed using the $\log_2$fold-change ranked sensitive and tolerant genes overlapped in each screen (DHA and BTZ). To access the enrichment, we used a database created from the latest curated *P. falciparum* Gene Ontology (GO) and Malaria Parasite Metabolic Pathways (MPMP) (http://mpmp.huji.ac.il/) available at the time of analysis, by Fast Gene Set Enrichment Analysis (FGSEA) v.4.2 (98) (Data Set S3).

Real-time quantitative reverse transcription-PCR gene expression. Real-time quantitative reverse transcription-PCR (qRT-PCR) was performed using gene-specific primers to both of the nearest genes to

the *piggyBac* insertion site in the *pB*104 mutant: genes related to StAR-related lipid transfer (PF3D7_0104200) and UBP1 (PF3D7_0104300) (Fig. S5). The PF3D7_071770 (seryl-tRNA synthetase) gene was used as an endogenous control. To validate the RNA-seq gene expression, total RNA of NF54 and *pB*104 lines was first extracted from ring-synchronized parasite cultures at time point zero (T0) and time point 96 h (T96), using the TRIzol-chloroform method as described previously. First-strand cDNA synthesis was carried out with 500 ng of each sample using oligo(dT)-primed reverse transcription with SuperScript II reverse transcriptase (Invitrogen) according to the manufacturer's instructions. The cDNA was then used as a template for real-time quantitative PCR (qPCR) using Luna Universal qPCR master mix (New England BioLab catalog no. M3003) according to the manufacturer's instructions. The threshold cycle ($\Delta\Delta C_T$) method was used to analyze the relative changes in expression level for each gene, using T0 as a calibrator sample (99). All qPCRs were performed in triplicates. The following primers were used for qPCR: (i) for the StAR-related lipid transfer gene (PF3D7_0104200), forward primer AGAAGAATCTCTTGAGACTGCTGCT and reverse primer CTCCCTTCTGCTTCTGCTTGAGC; (ii) for the UBP1 gene (PF3D7_0104300), forward primer TGCCTTAAAGTGGAATGAAATTATATCCC and reverse primer GTCCTGATGATGCTGATATCCCACC; and (iii) for the seryl-tRNA synthetase gene (PF3D7_0717700), forward primer AAGTAGCAGGTCATCGTGGTT and reverse primer TTCGGCACATTCTTCCATAA.

Whole-genome sequence analysis. Whole-genome sequence analysis was performed to confirm the *piggyBac* insertion location and to search for eventual additional mutation, comparing NF54 with *pB*104 genomes. Genomic DNA of NF54 and *pB*104 were used for whole-genome sequencing, using the Illumina NextSeq550, Mid Out-put kit. Raw reads were mapped to the *Plasmodium falciparum* 3D7 reference genome (PlasmoDB v.58) using mapped reads from HISAT2 (93). The sequence alignment data were then postprocessed using SAMtools (94). The Integrative Genomics Viewer (IGV) (100) was used to visualize reads mapped at the *piggyBac* insertion site (Fig. S4B). Bedtools (v.2.28.0) (101) was used to comparative analysis to evaluate the presence of eventual additional mutations, such as SNPs and indels.

Data availability. Raw QIseq data sets generated for this study were deposited to the European Nucleotide Archive under study accession code ERP114305 and are presented as follows in the format sample ID primer 3′, primer 5′, accession no.: T0_NoDrug_1_1_3, T0_NoDrug_1_1_5, ERS3788434; T0_NoDrug_1_2_3, T0_NoDrug_1_2_5, ERS3788441; T0_NoDrug_2_1_3, T0_NoDrug_2_1_5, ERS3788447; T0_NoDrug_2_2_3, T0_NoDrug_2_2_5, ERS3788457; T2_NoDrug_1_1_3, T2_NoDrug_1_1_5, ERS3788436; T2_NoDrug_1_2_3, T2_NoDrug_1_2_5, ERS3788442; T2_NoDrug_2_1_3, T2_NoDrug_2_1_5, ERS3788449; T2_NoDrug_2_2_3, T2_NoDrug_2_2_5, ERS3788458; T4_NoDrug_1_1_3, T4_NoDrug_1_1_5, ERS3788438; T4_NoDrug_1_2_3, T4_NoDrug_1_2_5, ERS3788444; T4_NoDrug_2_1_3, T4_NoDrug_2_1_5, ERS3788453; T4_NoDrug_2_2_3, T4_NoDrug_2_2_5, ERS3788460; T2_BTZ_IC25_1_1_3, T2_BTZ_IC25_1_1_5, ERS3788437; T2_BTZ_IC25_1_2_3, T2_BTZ_IC25_1_2_5, ERS3788446; T2_DHA_IC25_2_1_3, T2_DHA_IC25_2_1_5, ERS3788450; and T2_DHA_IC25_2_2_3, T2_DHA_IC25_2_2_5, ERS3788461.

Original QIseq read mapping data are provide in Data Set S1, Tab 2.

RNA-seq data generated for this study have been deposited in the NCBI Gene Expression Omnibus (GEO) database under accession no. GSE188542. Processed RNA-seq data are provided in Data Sets S4 and S5.

Whole-genome sequence data generated for this study have been deposited in the NCBI Sequence Read Archive (SRA) database under accession no. SAMN31408180 for wild-type NF54 and SAMN31408181 for *pB*104.

SUPPLEMENTAL MATERIAL

Supplemental material is available online only.
SUPPLEMENTAL FILE 1, PDF file, 4.6 MB.
SUPPLEMENTAL FILE 10, XLSX file, 0.02 MB.
SUPPLEMENTAL FILE 2, PDF file, 0.1 MB.
SUPPLEMENTAL FILE 3, XLSX file, 0.1 MB.
SUPPLEMENTAL FILE 4, XLSX file, 0.4 MB.
SUPPLEMENTAL FILE 5, XLSX file, 0.01 MB.
SUPPLEMENTAL FILE 6, XLSX file, 2.2 MB.
SUPPLEMENTAL FILE 7, XLSX file, 2.2 MB.
SUPPLEMENTAL FILE 8, XLSX file, 0.8 MB.
SUPPLEMENTAL FILE 9, XLSX file, 0.01 MB.

ACKNOWLEDGMENTS

REFERENCES

1. WHO. 2021. World malaria report 2021. https://www.who.int/teams/global-malaria-programme/reports/world-malaria-report-2021.

2. Ariey F, Witkowski B, Amaratunga C, Beghain J, Langlois A-C, Khim N, Kim S, Duru V, Bouchier C, Ma L, Lim P, Leang R, Duong S, Sreng S, Suon S, Chuor CM, Bout DM, Ménard S, Rogers WO, Genton B, Fandeur T, Miotto O, Ringwald P, Le Bras J, Berry A, Barale J-C, Fairhurst RM, Benoit-Vical F, Mercereau-Puijalon O, Ménard D. 2014. A molecular marker of artemisinin-resistant Plasmodium falciparum malaria. Nature 505:50–55. https://doi.org/10.1038/nature12876.

3. Takala-Harrison S, Jacob CG, Arze C, Cummings MP, Silva JC, Dondorp AM, Fukuda MM, Hien TT, Mayxay M, Noedl H, Nosten F, Kyaw MP, Nhien NTT, Imwong M, Bethell D, Se Y, Lon C, Tyner SD, Saunders DL, Ariey F, Mercereau-Puijalon O, Menard D, Newton PN, Khanthavong M, Hongvanthong B, Starzengruber P, Fuehrer H-P, Swoboda P, Khan WA, Phyo AP, Nyunt MM, Nyunt MH, Brown TS, Adams M, Pepin CS, Bailey J, Tan JC, Ferdig MT, Clark TG, Miotto O, MacInnis B, Kwiatkowski DP, White NJ, Ringwald P, Plowe CV. 2015. Independent emergence of artemisinin resistance mutations among Plasmodium falciparum in Southeast Asia. J Infect Dis 211:670–679. https://doi.org/10.1093/infdis/jiu491.

4. Miotto O, Amato R, Ashley EA, MacInnis B, Almagro-Garcia J, Amaratunga C, Lim P, Mead D, Oyola SO, Dhorda M, Imwong M, Woodrow C, Manske M, Stalker J, Drury E, Campino S, Amenga-Etego L, Thanh T-NN, Tran HT, Ringwald P, Bethell D, Nosten F, Phyo AP, Pukrittayakamee S, Chotivanich K, Chuor CM, Nguon C, Suon S, Sreng S, Newton PN, Mayxay M, Khanthavong M, Hongvanthong B, Htut Y, Han KT, Kyaw MP, Faiz MA, Fanello CI, Onyamboko M, Mokuolu OA, Jacob CG, Takala-Harrison S, Plowe CV, Day NP, Dondorp AM, Spencer CCA, McVean G, Fairhurst RM, White NJ, Kwiatkowski DP, et al. 2015. Genetic architecture of artemisinin-resistant Plasmodium falciparum. Nat Genet 47:226–234. https://doi.org/10.1038/ng.3189.

5. Duru V, Witkowski B, Ménard D. 2016. Plasmodium falciparum resistance to artemisinin derivatives and piperaquine: a major challenge for malaria elimination in Cambodia. Am J Trop Med Hyg 95:1228–1238. https://doi.org/10.4269/ajtmh.16-0234.

6. Chaorattanakawee S, Lon C, Jongsakul K, Gawee J, Sok S, Sundrakes S, Kong N, Thamnurak C, Chann S, Chattrakarn S, Praditpol C, Buathong N, Uthaimongkol N, Smith P, Sirisopana N, Huy R, Prom S, Fukuda MM, Bethell D, Walsh DS, Lanteri C, Saunders D. 2016. Ex vivo piperaquine resistance developed rapidly in Plasmodium falciparum isolates in northern Cambodia compared to Thailand. Malar J 15:519. https://doi.org/10.1186/s12936-016-1569-y.

7. Balikagala B, Fukuda N, Ikeda M, Katuro OT, Tachibana S-I, Yamauchi M, Opio W, Emoto S, Anywar DA, Kimura E, Palacpac NMQ, Odongo-Aginya EI, Ogwang M, Horii T, Mita T. 2021. Evidence of artemisinin-resistant malaria in Africa. N Engl J Med 385:1163–1171. https://doi.org/10.1056/NEJMoa2101746.

8. Lubell Y, Dondorp A, Guérin PJ, Drake T, Meek S, Ashley E, Day NPJ, White NJ, White LJ. 2014. Artemisinin resistance—modelling the potential human and economic costs. Malar J 13:452. https://doi.org/10.1186/1475-2875-13-452.

9. Klonis N, Crespo-Ortiz MP, Bottova I, Abu-Bakar N, Kenny S, Rosenthal PJ, Tilley L. 2011. Artemisinin activity against Plasmodium falciparum requires hemoglobin uptake and digestion. Proc Natl Acad Sci U S A 108:11405–11410. https://doi.org/10.1073/pnas.1104063108.

10. Gopalakrishnan AM, Kumar N. 2015. Antimalarial action of artesunate involves DNA damage mediated by reactive oxygen species. Antimicrob Agents Chemother 59:317–325. https://doi.org/10.1128/AAC.03663-14.

11. Combrinck JM, Mabotha TE, Ncokazi KK, Ambele MA, Taylor D, Smith PJ, Hoppe HC, Egan TJ. 2013. Insights into the role of heme in the mechanism of action of antimalarials. ACS Chem Biol 8:133–137. https://doi.org/10.1021/cb300454t.

12. Loup C, Lelièvre J, Benoit-Vical F, Meunier B. 2007. Trioxaquines and heme-artemisinin adducts inhibit the in vitro formation of hemozoin better than chloroquine. Antimicrob Agents Chemother 51:3768–3770. https://doi.org/10.1128/AAC.00239-07.

13. Ismail HM, Barton V, Phanchana M, Charoensutthivarakul S, Wong MHL, Hemingway J, Biagini GA, O'Neill PM, Ward SA. 2016. Artemisinin activity-based probes identify multiple molecular targets within the asexual stage of the malaria parasites Plasmodium falciparum 3D7. Proc Natl Acad Sci U S A 113:2080–2085. https://doi.org/10.1073/pnas.1600459113.

14. Jourdan J, Walz A, Matile H, Schmidt A, Wu J, Wang X, Dong Y, Vennerstrom JL, Schmidt RS, Wittlin S, Mäser P. 2019. Stochastic protein alkylation by antimalarial peroxides. ACS Infect Dis 5:2067–2075. https://doi.org/10.1021/acsinfecdis.9b00264.

15. Wang J, Zhang C-J, Chia WN, Loh CCY, Li Z, Lee YM, He Y, Yuan L-X, Lim TK, Liu M, Liew CX, Lee YQ, Zhang J, Lu N, Lim CT, Hua Z-C, Liu B, Shen H-M, Tan KSW, Lin Q. 2015. Haem-activated promiscuous targeting of artemisinin in Plasmodium falciparum. Nat Commun 6:10111. https://doi.org/10.1038/ncomms10111.

16. Bridgford JL, Xie SC, Cobbold SA, Pasaje CFA, Herrmann S, Yang T, Gillett DL, Dick LR, Ralph SA, Dogovski C, Spillman NJ, Tilley L. 2018. Artemisinin kills malaria parasites by damaging proteins and inhibiting the proteasome. Nat Commun 9:3801. https://doi.org/10.1038/s41467-018-06221-1.

17. Kirkman LA, Zhan W, Visone J, Dziedziech A, Singh PK, Fan H, Tong X, Bruzual I, Hara R, Kawasaki M, Imaeda T, Okamoto R, Sato K, Michino M, Alvaro EF, Guiang LF, Sanz L, Mota DJ, Govindasamy K, Wang R, Ling Y, Tumwebaze PK, Sukenick G, Shi L, Vendome J, Bhanot P, Rosenthal PJ, Aso K, Foley MA, Cooper RA, Kafsack B, Doggett JS, Nathan CF, Lin G. 2018. Antimalarial proteasome inhibitor reveals collateral sensitivity from intersubunit interactions and fitness cost of resistance. Proc Natl Acad Sci U S A 115:E6863–E6870. https://doi.org/10.1073/pnas.1806109115.

18. Dogovski C, Xie SC, Burgio G, Bridgford J, Mok S, McCaw JM, Chotivanich K, Kenny S, Gnädig N, Straimer J, Bozdech Z, Fidock DA, Simpson JA, Dondorp AM, Foote S, Klonis N, Tilley L. 2015. Targeting the cell stress response of Plasmodium falciparum to overcome artemisinin resistance. PLoS Biol 13:e1002132. https://doi.org/10.1371/journal.pbio.1002132.

19. Birnbaum J, Scharf S, Schmidt S, Jonscher E, Hoeijmakers WAM, Flemming S, Toenhake CG, Schmitt M, Sabitzki R, Bergmann B, Fröhlke U, Mesén-Ramírez P, Blancke Soares A, Herrmann H, Bártfai R, Spielmann T. 2020. A Kelch13-defined endocytosis pathway mediates artemisinin resistance in malaria parasites. Science 367:51–59. https://doi.org/10.1126/science.aax4735.

20. Henriques G, Martinelli A, Rodrigues L, Modrzynska K, Fawcett R, Houston DR, Borges ST, d'Alessandro U, Tinto H, Karema C, Hunt P, Cravo P. 2013. Artemisinin resistance in rodent malaria—mutation in the AP2 adaptor mu-chain suggests involvement of endocytosis and membrane protein trafficking. Malar J 12:118. https://doi.org/10.1186/1475-2875-12-118.

21. Henriques G, Hallett RL, Beshir KB, Gadalla NB, Johnson RE, Burrow R, van Schalkwyk DA, Sawa P, Omar SA, Clark TG, Bousema T, Sutherland CJ. 2014. Directional selection on the pfmdr1, pfcrt, pfubp1, and pfap2mu loci of Plasmodium falciparum in Kenyan children treated with ACT. J Infect Dis 210:2001–2008. https://doi.org/10.1093/infdis/jiu358.

22. Henriques G, van Schalkwyk DA, Burrow R, Warhurst DC, Thompson E, Baker DA, Fidock DA, Hallett R, Flueck C, Sutherland CJ. 2015. The Mu subunit of Plasmodium falciparum clathrin-associated adaptor protein 2 modulates in vitro parasite response to artemisinin and quinine. Antimicrob Agents Chemother 59:2540–2547. https://doi.org/10.1128/AAC.04067-14.

23. Demas AR, Sharma AI, Wong W, Early AM, Redmond S, Bopp S, Neafsey DE, Volkman SK, Hartl DL, Wirth DF. 2018. Mutations in Plasmodium falciparum actin-binding protein coronin confer reduced artemisinin susceptibility. Proc Natl Acad Sci U S A 115:12799–12804. https://doi.org/10.1073/pnas.1812317115.

24. Yuan W-C, Lee Y-R, Lin S-Y, Chang L-Y, Tan YP, Hung C-C, Kuo J-C, Liu C-H, Lin M-Y, Xu M, Chen ZJ, Chen R-H. 2014. K33-linked polyubiquitination of coronin 7 by Cul3-KLHL20 ubiquitin E3 ligase regulates protein trafficking. Mol Cell 54:586–600. https://doi.org/10.1016/j.molcel.2014.03.035.

25. Siddiqui FA, Cabrera M, Wang M, Brashear A, Kemirembe K, Wang Z, Miao J, Chookajorn T, Yang Z, Cao Y, Dong G, Rosenthal PJ, Cui L. 2018. Plasmodium falciparum falcipain-2a polymorphisms in Southeast Asia and their association with artemisinin resistance. J Infect Dis 218:434–442. https://doi.org/10.1093/infdis/jiy188.

26. Xie SC, Dogovski C, Hanssen E, Chiu F, Yang T, Crespo MP, Stafford C, Batinovic S, Teguh S, Charman S, Klonis N, Tilley L. 2016. Haemoglobin degradation underpins the sensitivity of early ring stage Plasmodium falciparum to artemisinins. J Cell Sci 129:406–416. https://doi.org/10.1242/jcs.178830.

27. Rocamora F, Zhu L, Liong KY, Dondorp A, Miotto O, Mok S, Bozdech Z. 2018. Oxidative stress and protein damage responses mediate artemisinin resistance in malaria parasites. PLoS Pathog 14:e1006930. https://doi.org/10.1371/journal.ppat.1006930.

28. Vaid A, Ranjan R, Smythe WA, Hoppe HC, Sharma P. 2010. PfPI3K, a phosphatidylinositol-3 kinase from Plasmodium falciparum, is exported to the host erythrocyte and is involved in hemoglobin trafficking. Blood 115:2500–2507. https://doi.org/10.1182/blood-2009-08-238972.

29. Mbengue A, Bhattacharjee S, Pandharkar T, Liu H, Estiu G, Stahelin RV, Rizk SS, Njimoh DL, Ryan Y, Chotivanich K, Nguon C, Ghorbal M, Lopez-Rubio J-J, Pfrender M, Emrich S, Mohandas N, Dondorp AM, Wiest O,

Haldar K. 2015. A molecular mechanism of artemisinin resistance in Plasmodium falciparum malaria. Nature 520:683–687. https://doi.org/10.1038/nature14412.

30. Bonnet M, van den Broek I, van Herp M, Urrutia PPP, van Overmeir C, Kyomuhendo J, Ndosimao CN, Ashley E, Guthmann J-P. 2009. Varying efficacy of artesunate+amodiaquine and artesunate+sulphadoxine-pyrimethamine for the treatment of uncomplicated falciparum malaria in the Democratic Republic of Congo: a report of two in-vivo studies. Malar J 8:192. https://doi.org/10.1186/1475-2875-8-192.

31. Shoemaker RH. 2006. The NCI60 human tumour cell line anticancer drug screen. Nat Rev Cancer 6:813–823. https://doi.org/10.1038/nrc1951.

32. Young J, Dominicus C, Wagener J, Butterworth S, Ye X, Kelly G, Ordan M, Saunders B, Instrell R, Howell M, Stewart A, Treeck M. 2019. A CRISPR platform for targeted in vivo screens identifies Toxoplasma gondii virulence factors in mice. Nat Commun 10:3963. https://doi.org/10.1038/s41467-019-11855-w.

33. Gomes AR, Bushell E, Schwach F, Girling G, Anar B, Quail MA, Herd C, Pfander C, Modrzynska K, Rayner JC, Billker O. 2015. A genome-scale vector resource enables high-throughput reverse genetic screening in a malaria parasite. Cell Host Microbe 17:404–413. https://doi.org/10.1016/j.chom.2015.01.014.

34. Stanway RR, Bushell E, Chiappino-Pepe A, Roques M, Sanderson T, Franke-Fayard B, Caldelari R, Golomingi M, Nyonda M, Pandey V, Schwach F, Chevalley S, Ramesar J, Metcalf T, Herd C, Burda P-C, Rayner JC, Soldati-Favre D, Janse CJ, Hatzimanikatis V, Billker O, Heussler VT. 2019. Genome-scale identification of essential metabolic processes for targeting the Plasmodium liver stage. Cell 179:1112–1128.e26. https://doi.org/10.1016/j.cell.2019.10.030.

35. Tang Y, Meister TR, Walczak M, Pulkoski-Gross MJ, Hari SB, Sauer RT, Amberg-Johnson K, Yeh E. 2019. A mutagenesis screen for essential plastid biogenesis genes in human malaria parasites. PLoS Biol 17:e3000136. https://doi.org/10.1371/journal.pbio.3000136.

36. Zhang M, Wang C, Oberstaller J, Thomas P, Otto TD, Casandra D, Boyapalle S, Adapa SR, Xu S, Button-Simons K, Mayho M, Rayner JC, Ferdig MT, Jiang RHY, Adams JH. 2021. The apicoplast link to fever-survival and artemisinin-resistance in the malaria parasite. Nat Commun 12:4563. https://doi.org/10.1038/s41467-021-24814-1.

37. Pradhan A, Siwo GH, Singh N, Martens B, Balu B, Button-Simons KA, Tan A, Zhang M, Udenze KO, Jiang RHY, Ferdig MT, Adams JH, Kyle DE. 2015. Chemogenomic profiling of Plasmodium falciparum as a tool to aid antimalarial drug discovery. Sci Rep 5:15930. https://doi.org/10.1038/srep15930.

38. Van Voorhis WC, Adams JH, Adelfio R, Ahyong V, Akabas MH, Alano P, Alday A, Alemán Resto Y, Alsibaee A, Alzualde A, Andrews KT, Avery SV, Avery VM, Ayong L, Baker M, Baker S, Ben Mamoun C, Bhatia S, Bickle Q, Bounaadja L, Bowling T, Bosch J, Boucher LE, Boyom FF, Brea J, Brennan M, Burton A, Caffrey CR, Camarda G, Carrasquilla M, Carter D, Belen Cassera M, Chih-Chien Cheng K, Chindaudomsate W, Chubb A, Colon BL, Colón-López DD, Corbett Y, Crowther GJ, Cowan N, D'Alessandro S, Le Dang N, Delves M, DeRisi JL, Du AY, Duffy S, Abd El-Salam El-Sayed S, Ferdig MT, Fernández Robledo JA, Fidock DA, et al. 2016. Open source drug discovery with the Malaria Box compound collection for neglected diseases and beyond. PLoS Pathog 12:e1005763. https://doi.org/10.1371/journal.ppat.1005763.

39. Zhang M, Wang C, Otto TD, Oberstaller J, Liao X, Adapa SR, Udenze K, Bronner IF, Casandra D, Mayho M, Brown J, Li S, Swanson J, Rayner JC, Jiang RHY, Adams JH. 2018. Uncovering the essential genes of the human malaria parasite Plasmodium falciparum by saturation mutagenesis. Science 360:eaap7847. https://doi.org/10.1126/science.aap7847.

40. Rosenthal MR, Ng CL. 2020. Plasmodium falciparum artemisinin resistance: the effect of heme, protein damage, and parasite cell stress response. ACS Infect Dis 6:1599–1614. https://doi.org/10.1021/acsinfecdis.9b00527.

41. Bronner IF, Otto TD, Zhang M, Udenze K, Wang C, Quail MA, Jiang RH, Adams JH, Rayner JC. 2016. Quantitative insertion-site sequencing (QIseq) for high throughput phenotyping of transposon mutants. Genome Res 26:980–989. https://doi.org/10.1101/gr.200279.115.

42. Bushell E, Gomes AR, Sanderson T, Anar B, Girling G, Herd C, Metcalf T, Modrzynska K, Schwach F, Martin RE, Mather MW, McFadden GI, Parts L, Rutledge GG, Vaidya AB, Wengelnik K, Rayner JC, Billker O. 2017. Functional profiling of a Plasmodium genome reveals an abundance of essential genes. Cell 170:260–272.e8. https://doi.org/10.1016/j.cell.2017.06.030.

43. Ng CL, Fidock DA, Bogyo M. 2017. Protein degradation systems as antimalarial therapeutic targets. Trends Parasitol 33:731–743. https://doi.org/10.1016/j.pt.2017.05.009.

44. Yang T, Yeoh LM, Tutor MV, Dixon MW, McMillan PJ, Xie SC, Bridgford JL, Gillett DL, Duffy MF, Ralph SA, McConville MJ, Tilley L, Cobbold SA. 2019. Decreased K13 abundance reduces hemoglobin catabolism and proteotoxic stress, underpinning artemisinin resistance. Cell Rep 29:2917–2928.e5. https://doi.org/10.1016/j.celrep.2019.10.095.

45. Tsujishita Y, Hurley JH. 2000. Structure and lipid transport mechanism of a StAR-related domain. Nat Struct Biol 7:408–414. https://doi.org/10.1038/75192.

46. Soccio RE, Breslow JL. 2003. StAR-related lipid transfer (START) proteins: mediators of intracellular lipid metabolism. J Biol Chem 278:22183–22186. https://doi.org/10.1074/jbc.R300003200.

47. Alpy F, Tomasetto C. 2005. Give lipids a START: the StAR-related lipid transfer (START) domain in mammals. J Cell Sci 118:2791–2801. https://doi.org/10.1242/jcs.02485.

48. Ramakrishnan S, Serricchio M, Striepen B, Bütikofer P. 2013. Lipid synthesis in protozoan parasites: a comparison between kinetoplastids and apicomplexans. Prog Lipid Res 52:488–512. https://doi.org/10.1016/j.plipres.2013.06.003.

49. Hill RJ, Ringel A, Knuepfer E, Moon RW, Blackman MJ, van Ooij C. 2016. Regulation and essentiality of the StAR-related lipid transfer (START) domain-containing phospholipid transfer protein PFA0210c in malaria parasites. J Biol Chem 291:24280–24292. https://doi.org/10.1074/jbc.M116.740506.

50. van Ooij C, Withers-Martinez C, Ringel A, Cockcroft S, Haldar K, Blackman MJ. 2013. Identification of a Plasmodium falciparum phospholipid transfer protein. J Biol Chem 288:31971–31983. https://doi.org/10.1074/jbc.M113.474189.

51. Beaumelle BD, Vial HJ. 1988. Correlation of the efficiency of fatty acid derivatives in suppressing Plasmodium falciparum growth in culture with their inhibitory effect on acyl-CoA synthetase activity. Mol Biochem Parasitol 28:39–42. https://doi.org/10.1016/0166-6851(88)90177-6.

52. Waller RF, Ralph SA, Reed MB, Su V, Douglas JD, Minnikin DE, Cowman AF, Besra GS, McFadden GI. 2003. A type II pathway for fatty acid biosynthesis presents drug targets in Plasmodium falciparum. Antimicrob Agents Chemother 47:297–301. https://doi.org/10.1128/AAC.47.1.297-301.2003.

53. Matesanz F, Téllez MM, Alcina A. 2003. The Plasmodium falciparum fatty acyl-CoA synthetase family (PfACS) and differential stage-specific expression in infected erythrocytes. Mol Biochem Parasitol. 126109–126112. https://doi.org/10.1016/s0166-6851(02)00242-6.

54. Lee SH, Stephens JL, Englund PT. 2007. A fatty-acid synthesis mechanism specialized for parasitism. Nat Rev Microbiol 5:287–297. https://doi.org/10.1038/nrmicro1617.

55. Chen N, LaCrue AN, Teuscher F, Waters NC, Gatton ML, Kyle DE, Cheng Q. 2014. Fatty acid synthesis and pyruvate metabolism pathways remain active in dihydroartemisinin-induced dormant ring stages of Plasmodium falciparum. Antimicrob Agents Chemother 58:4773–4781. https://doi.org/10.1128/AAC.02647-14.

56. Shears MJ, Botte CY, McFadden GI. 2015. Fatty acid metabolism in the Plasmodium apicoplast: drugs, doubts and knockouts. Mol Biochem Parasitol 199:34–50. https://doi.org/10.1016/j.molbiopara.2015.03.004.

57. Hayakawa EH, Yamaguchi K, Mori M, Nardone G. 2020. Real-time cholesterol sorting in Plasmodium falciparum-erythrocytes as revealed by 3D label-free imaging. Sci Rep 10:2794. https://doi.org/10.1038/s41598-020-59552-9.

58. Hayakawa EH, Kato H, Nardone GA, Usukura J. 2021. A prospective mechanism and source of cholesterol uptake by Plasmodium falciparum-infected erythrocytes co-cultured with HepG2 cells. Parasitol Int 80:102179. https://doi.org/10.1016/j.parint.2020.102179.

59. Hiller NL, Bhattacharjee S, van Ooij C, Liolios K, Harrison T, Lopez-Estraño C, Haldar K. 2004. A host-targeting signal in virulence proteins reveals a secretome in malarial infection. Science 306:1934–1937. https://doi.org/10.1126/science.1102737.

60. van Ooij C, Tamez P, Bhattacharjee S, Hiller NL, Harrison T, Liolios K, Kooij T, Ramesar J, Balu B, Adams J, Waters AP, Janse CJ, Haldar K. 2008. The malaria secretome: from algorithms to essential function in blood stage infection. PLoS Pathog 4:e1000084. https://doi.org/10.1371/journal.ppat.1000084.

61. Boddey JA, Carvalho TG, Hodder AN, Sargeant TJ, Sleebs BE, Marapana D, Lopaticki S, Nebl T, Cowman AF. 2013. Role of plasmepsin V in export of diverse protein families from the Plasmodium falciparum exportome. Traffic 14:532–550. https://doi.org/10.1111/tra.12053.

62. Marti M, Good RT, Rug M, Knuepfer E, Cowman AF. 2004. Targeting malaria virulence and remodeling proteins to the host erythrocyte. Science 306:1930–1933. https://doi.org/10.1126/science.1102452.

63. Heiber A, Kruse F, Pick C, Grüring C, Flemming S, Oberli A, Schoeler H, Retzlaff S, Mesén-Ramírez P, Hiss JA, Kadekoppala M, Hecht L, Holder AA, Gilberger T-W, Spielmann T. 2013. Identification of new PNEPs indicates a substantial non-PEXEL exportome and underpins common features in

Plasmodium falciparum protein export. PLoS Pathog 9:e1003546. https://doi.org/10.1371/journal.ppat.1003546.

64. Mok S, Stokes BH, Gnädig NF, Ross LS, Yeo T, Amaratunga C, Allman E, Solyakov L, Bottrill AR, Tripathi J, Fairhurst RM, Llinás M, Bozdech Z, Tobin AB, Fidock DA. 2021. Artemisinin-resistant K13 mutations rewire Plasmodium falciparum's intra-erythrocytic metabolic program to enhance survival. Nat Commun 12:530. https://doi.org/10.1038/s41467-020-20805-w.

65. Cohen A, Dumetre A, Azas N. 2013. A decade of Plasmodium metabolic pathways of therapeutic interest to develop new selective antimalarial drugs. Mini Rev Med Chem 13:1340–1347. https://doi.org/10.2174/13895575113139990060.

66. Zhu L, Tripathi J, Rocamora FM, Miotto O, van der Pluijm R, Voss TS, Mok S, Kwiatkowski DP, Nosten F, Day NPJ, White NJ, Dondorp AM, Bozdech Z, Tracking Resistance to Artemisinin Collaboration I. 2018. The origins of malaria artemisinin resistance defined by a genetic and transcriptomic background. Nat Commun 9:5158. https://doi.org/10.1038/s41467-018-07588-x.

67. Imlay L, Odom AR. 2014. Isoprenoid metabolism in apicomplexan parasites. Curr Clin Microbiol Rep 1:37–50. https://doi.org/10.1007/s40588-014-0006-7.

68. Shunmugam S, Arnold C-S, Dass S, Katris NJ, Botté CY. 2022. The flexibility of Apicomplexa parasites in lipid metabolism. PLoS Pathog 18:e1010313. https://doi.org/10.1371/journal.ppat.1010313.

69. Jonsdottir TK, Gabriela M, Crabb BS, de Koning-Ward TF, Gilson PR. 2021. Defining the essential exportome of the malaria parasite. Trends Parasitol 37:664–675. https://doi.org/10.1016/j.pt.2021.04.009.

70. Kats LM, Fernandez KM, Glenister FK, Herrmann S, Buckingham DW, Siddiqui G, Sharma L, Bamert R, Lucet I, Guillotte M, Mercereau-Puijalon O, Cooke BM. 2014. An exported kinase (FIKK4.2) that mediates virulence-associated changes in Plasmodium falciparum-infected red blood cells. Int J Parasitol 44:319–328. https://doi.org/10.1016/j.ijpara.2014.01.003.

71. Cobb DW, Florentin A, Fierro MA, Krakowiak M, Moore JM, Muralidharan V. 2017. The exported chaperone PfHsp70x is dispensable for the Plasmodium falciparum intraerythrocytic life cycle. mSphere 2:e00363-17. https://doi.org/10.1128/mSphere.00363-17.

72. Külzer S, Charnaud S, Dagan T, Riedel J, Mandal P, Pesce ER, Blatch GL, Crabb BS, Gilson PR, Przyborski JM. 2012. Plasmodium falciparum-encoded exported hsp70/hsp40 chaperone/co-chaperone complexes within the host erythrocyte. Cell Microbiol 14:1784–1795. https://doi.org/10.1111/j.1462-5822.2012.01840.x.

73. Alpy F, Tomasetto C. 2014. START ships lipids across interorganelle space. Biochimie 96:85–95. https://doi.org/10.1016/j.biochi.2013.09.015.

74. Zhu L, van der Pluijm RW, Kucharski M, Nayak S, Tripathi J, White NJ, Day NPJ, Faiz A, Phyo AP, Amaratunga C, Lek D, Ashley EA, Nosten F, Smithuis F, Ginsburg H, von Seidlein L, Lin K, Imwong M, Chotivanich K, Mayxay M, Dhorda M, Nguyen HC, Nguyen TNT, Miotto O, Newton PN, Jittamala P, Tripura R, Pukrittayakamee S, Peto TJ, Hien TT, Dondorp AM, Bozdech Z. 2022. Artemisinin resistance in the malaria parasite, Plasmodium falciparum, originates from its initial transcriptional response. Commun Biol 5:274. https://doi.org/10.1038/s42003-022-03215-0.

75. Beck JR, Muralidharan V, Oksman A, Goldberg DE. 2014. PTEX component HSP101 mediates export of diverse malaria effectors into host erythrocytes. Nature 511:592–595. https://doi.org/10.1038/nature13574.

76. Charnaud SC, Kumarasingha R, Bullen HE, Crabb BS, Gilson PR. 2018. Knockdown of the translocon protein EXP2 in Plasmodium falciparum reduces growth and protein export. PLoS One 13:e0204785. https://doi.org/10.1371/journal.pone.0204785.

77. Garten M, Nasamu AS, Niles JC, Zimmerberg J, Goldberg DE, Beck JR. 2018. EXP2 is a nutrient-permeable channel in the vacuolar membrane of Plasmodium and is essential for protein export via PTEX. Nat Microbiol 3:1090–1098. https://doi.org/10.1038/s41564-018-0222-7.

78. Mok S, Ashley EA, Ferreira PE, Zhu L, Lin Z, Yeo T, Chotivanich K, Imwong M, Pukrittayakamee S, Dhorda M, Nguon C, Lim P, Amaratunga C, Suon S, Hien TT, Htut Y, Faiz MA, Onyamboko MA, Mayxay M, Newton PN, Tripura R, Woodrow CJ, Miotto O, Kwiatkowski DP, Nosten F, Day NPJ, Preiser PR, White NJ, Dondorp AM, Fairhurst RM, Bozdech Z. 2015. Drug resistance. Population transcriptomics of human malaria parasites reveals the mechanism of artemisinin resistance. Science 347:431–435. https://doi.org/10.1126/science.1260403.

79. Gupta DK, Patra AT, Zhu L, Gupta AP, Bozdech Z. 2016. DNA damage regulation and its role in drug-related phenotypes in the malaria parasites. Sci Rep 6:23603. https://doi.org/10.1038/srep23603.

80. Zhang M, Gallego-Delgado J, Fernandez-Arias C, Waters NC, Rodriguez A, Tsuji M, Wek RC, Nussenzweig V, Sullivan WJ. 2017. Inhibiting the Plasmodium eIF2alpha kinase PK4 prevents artemisinin-induced latency. Cell Host Microbe 22:766–776.e4. https://doi.org/10.1016/j.chom.2017.11.005.

81. Gibbons J, Button-Simons KA, Adapa SR, Li S, Pietsch M, Zhang M, Liao X, Adams JH, Ferdig MT, Jiang RHY. 2018. Altered expression of K13 disrupts DNA replication and repair in Plasmodium falciparum. BMC Genomics 19:849. https://doi.org/10.1186/s12864-018-5207-7.

82. Beaumelle BD, Vial HJ. 1988. Acyl-CoA synthetase activity in Plasmodium knowlesi-infected erythrocytes displays peculiar substrate specificities. Biochim Biophys Acta 958:1–9. https://doi.org/10.1016/0005-2760(88)90239-1.

83. Matesanz F, Tellez M, Alcina A. 2003. The Plasmodium falciparum fatty acyl-CoA synthetase family (PfACS) and differential stage-specific expression in infected erythrocytes. Mol Biochem Parasitol 126:109–112. https://doi.org/10.1016/s0166-6851(02)00242-6.

84. Tellez M, Matesanz F, Alcina A. 2003. The C-terminal domain of the Plasmodium falciparum acyl-CoA synthetases PfACS1 and PfACS3 functions as ligand for ankyrin. Mol Biochem Parasitol 129:191–198. https://doi.org/10.1016/s0166-6851(03)00123-3.

85. Oberstaller J, Zoungrana L, Bannerman CD, Jahangiri S, Dwivedi A, Silva JC, Adams JH, Takala-Harrison S. 2021. Integration of population and functional genomics to understand mechanisms of artemisinin resistance in Plasmodium falciparum. Int J Parasitol Drugs Drug Resist 16:119–128. https://doi.org/10.1016/j.ijpddr.2021.05.006.

86. Salcedo-Sora JE, Caamano-Gutierrez E, Ward SA, Biagini GA. 2014. The proliferating cell hypothesis: a metabolic framework for Plasmodium growth and development. Trends Parasitol 30:170–175. https://doi.org/10.1016/j.pt.2014.02.001.

87. Takano R, Kozuka-Hata H, Kondoh D, Bochimoto H, Oyama M, Kato K. 2019. A high-resolution map of SBP1 interactomes in Plasmodium falciparum-infected erythrocytes. iScience 19:703–714. https://doi.org/10.1016/j.isci.2019.07.035.

88. Krishnan KM, Williamson KC. 2018. The proteasome as a target to combat malaria: hits and misses. Transl Res 198:40–47. https://doi.org/10.1016/j.trsl.2018.04.007.

89. Ng CS, Sinha A, Aniweh Y, Nah Q, Babu IR, Gu C, Chionh YH, Dedon PC, Preiser PR. 2018. tRNA epitranscriptomics and biased codon are linked to proteome expression in Plasmodium falciparum. Mol Syst Biol 14:e8009. https://doi.org/10.15252/msb.20178009.

90. Sorber K, Dimon MT, DeRisi JL. 2011. RNA-Seq analysis of splicing in Plasmodium falciparum uncovers new splice junctions, alternative splicing and splicing of antisense transcripts. Nucleic Acids Res 39:3820–3835. https://doi.org/10.1093/nar/gkq1223.

91. de Vries PJ, Dien TK. 1996. Clinical pharmacology and therapeutic potential of artemisinin and its derivatives in the treatment of malaria. Drugs 52:818–836. https://doi.org/10.2165/00003495-199652060-00004.

92. Sibley CH. 2013. Tracking artemisinin resistance in Plasmodium falciparum. Lancet Infect Dis 13:999–1000. https://doi.org/10.1016/S1473-3099(13)70260-3.

93. Kim D, Paggi JM, Park C, Bennett C, Salzberg SL. 2019. Graph-based genome alignment and genotyping with HISAT2 and HISAT-genotype. Nat Biotechnol 37:907–915. https://doi.org/10.1038/s41587-019-0201-4.

94. Li H, Handsaker B, Wysoker A, Fennell T, Ruan J, Homer N, Marth G, Abecasis G, Durbin R, 1000 Genome Project Data Processing Subgroup. 2009. The Sequence Alignment/Map format and SAMtools. Bioinformatics 25:2078–2079. https://doi.org/10.1093/bioinformatics/btp352.

95. Liao Y, Smyth GK, Shi W. 2014. featureCounts: an efficient general purpose program for assigning sequence reads to genomic features. Bioinformatics 30:923–930. and https://doi.org/10.1093/bioinformatics/btt656.

96. Oberstaller J. 2022. pfGO: P. falciparum functional enrichment analysis tools. https://github.com/oberstal/pfGO.

97. Alexa A, Rahnenfuhrer J. 2019. topGO: Enrichment Analysis for Gene Ontology. https://rdrr.io/bioc/topGO/.

98. Korotkevich G, Sukhov V, Sergushichev A. 2019. Fast gene set enrichment analysis. bioRxiv https://www.biorxiv.org/content/10.1101/060012v2.full.pdf.

99. Livak KJ, Schmittgen TD. 2001. Analysis of relative gene expression data using real-time quantitative PCR and the 2(T)(-Delta Delta C) method. Methods 25:402–408. https://doi.org/10.1006/meth.2001.1262.

100. Robinson JT, Thorvaldsdóttir H, Winckler W, Guttman M, Lander ES, Getz G, Mesirov JP. 2011. Integrative genomics viewer. Nat Biotechnol 29:24–26. https://doi.org/10.1038/nbt.1754.

101. Quinlan AR, Hall IM. 2010. BEDTools: a flexible suite of utilities for comparing genomic features. Bioinformatics 26:841–842. https://doi.org/10.1093/bioinformatics/btq033.